Neoantigen-specific CD4+ tumor-infiltrating lymphocytes are potent effectors identified within adoptive cell therapy products for metastatic melanoma patients

MacLean S. Hall [ORCID],[1,2] Jamie K. Teer,[3] Xiaoqing Yu,[3] Holly Branthoover,[1] Sebastian Snedal [ORCID],[1] Madeline Rodriguez-Valentin,[1] Luz Nagle,[1] Ellen Scott,[1] Ben Schachner [ORCID],[1] Patrick Innamarato,[1] Amy M. Hall,[1] Jamie Blauvelt,[1] Carolyn J. Rich,[4] Allison D. Richards,[4] Jake Ceccarelli,[5] TJ Langer,[5] Sean J. Yoder,[6] Matthew S. Beatty,[1] Cheryl A. Cox,[7] Jane L. Messina,[8] Daniel Abate-Daga,[1] James J. Mule [ORCID],[1] John E. Mullinax [ORCID],[1,9] Amod A. Sarnaik [ORCID],[1,4] Shari Pilon-Thomas[1]

For numbered affiliations see end of article.

Correspondence to
Dr Shari Pilon-Thomas;
shari.pilon-thomas@moffitt.org

ABSTRACT

Background Adoptive cell therapy (ACT) with tumor-infiltrating lymphocytes (TILs) is a promising immunotherapeutic approach for patients with advanced solid tumors. While numerous advances have been made, the contribution of neoantigen-specific CD4+T cells within TIL infusion products remains underexplored and therefore offers a significant opportunity for progress.

Methods We analyzed infused TIL products from metastatic melanoma patients previously treated with ACT for the presence of neoantigen-specific T cells. TILs were enriched on reactivity to neoantigen peptides derived and prioritized from patient sample-directed mutanome analysis. Enriched TILs were further investigated to establish the clonal neoantigen response with respect to function, transcriptomics, and persistence following ACT.

Results We discovered that neoantigen-specific TIL clones were predominantly CD4+ T cells and were present in both therapeutic responders and non-responders. CD4+ TIL demonstrated an effector T cell response with cytotoxicity toward autologous tumor in a major histocompatibility complex class II-dependent manner. These results were validated by paired TCR and single cell RNA sequencing, which elucidated transcriptomic profiles distinct to neoantigen-specific CD4+ TIL.

Conclusions Despite methods which often focus on CD8+T cells, our study supports the importance of prospective identification of neoantigen-specific CD4+ T cells within TIL products as they are a potent source of tumor-specific effectors. We further advocate for the inclusion of neoantigen-specific CD4+ TIL in future ACT protocols as a strategy to improve antitumor immunity.

INTRODUCTION

Immunotherapy has revolutionized the expected outcomes for patients with cancer due to the potential for durable, complete

WHAT IS ALREADY KNOWN ON THIS TOPIC

⇒ Adoptive cell therapy (ACT) with tumor-infiltrating lymphocytes (TIL) is a highly effective immunotherapy, but prior studies have predominantly focused on CD8+ T cell activity in this setting while the potential contribution of CD4+ TIL remains underexplored.

WHAT THIS STUDY ADDS

⇒ Here, we identified neoantigen-specific CD4+ T cell clones present in the TIL infusion product of previously treated metastatic melanoma patients. Functional and transcriptomic clonal analysis determined that these CD4+ TIL were distinct neoantigen-specific effectors capable of an antitumor immune response.

HOW THIS STUDY MIGHT AFFECT RESEARCH, PRACTICE AND/OR POLICY

⇒ These data support the proactive identification of neoantigen-specific CD4+ T cells for inclusion in ACT and other immunotherapeutic approaches as a means to improve efficacy.

clinical responses, yet there remains a dire need to expand and improve on these therapies. In metastatic melanoma, adoptive cell therapy (ACT) with tumor-infiltrating lymphocytes (TILs) has resulted in objective response rates ranging from 28% to 56%.[1–4] Most current TIL production strategies focus on the expansion and selection of tumor-reactive CD8+ T cells for infusion. However, recent evidence suggests an expanded role for CD4+ T cells in antitumor immunity, warranting further investigation into the

function and potential efficacy of this underexplored TIL population in ACT.[5–8]

Shared antigen and neoantigen-specific CD4^{+} T cells have been detected in the peripheral blood and within the tumor microenvironment across multiple cancer types, indicating their availability and potential utility in the immunotherapeutic setting.[9–13] Several notable studies have demonstrated the efficacy of antigen-specific CD4^{+} T cells in ACT, including complete responses (CR) in advanced cancers following infusion of highly potent CD4-dominant T cell products. These clinical responses were marked by CD4^{+} effector T cells with pleiotropic functionality including cytokine production and long-term persistence, resulting in overall reduced tumor burden.[14–18] While these reports suggested that antigen-specific CD4^{+} T cells were effective mediators of the anti-tumor immune response, the prevalence, profile, and mechanism of action remain unclear.

CD4^{+} T cells are integral orchestrators of both the primary and secondary immune responses, yet have been classically considered helpers.[19–22] A diverse and plastic population, CD4^{+} T cells are capable of a polyfunctional response on recognition of cognate peptide presented on major histocompatibility complex (MHC) class II molecules on antigen presenting cells (APCs) or tumor cells directly.[23 24] Recent reports have demonstrated that CD4^{+} T cells possess direct and indirect effector functions, including pleiotropic cytokine production and tumor cytolytic capacity dependent on MHC class II-directed cell-to-cell interactions resulting in T cell degranulation.[25–29] The maintenance of these antigen-specific CD4^{+} T cells in vivo is critical to therapeutic efficacy and has been demonstrated in long-term responders following ACT.[30–33] The advent of single cell RNA sequencing (scRNASeq) has improved the depth and insight into neoantigen-specific T cells dramatically, uncovering genetic signatures and modules which demarcate this critical population.[34–39]

Here, we report the identification and characterization of neoantigen-specific CD4^{+} T cell clones present within the TIL infusion product from previously treated melanoma patients. Through a series of case studies, we demonstrated that these neoantigen-specific CD4^{+} TIL were highly activated in response to tumor antigens and exhibited MHC Class II-mediated cytotoxicity. We then used T cell receptor (TCR) sequencing and scRNASeq to validate the in vitro and in vivo functional activity and further contextualize these neoantigen-specific CD4^{+} TIL. Overall, these data support an important role for neoantigen-specific CD4^{+} TIL and advocate for their inclusion in ACT.

MATERIALS AND METHODS
Patients and patient samples
Retrospective analysis was performed on TIL, peripheral blood mononuclear cells (PBMC), and excess tumor material derived from metastatic melanoma patients previously treated with ACT at Moffitt Cancer Center (MCC) as described under the Study approval section. As necessary, TILs were propagated by the Rapid Expansion Protocol (REP), consistent with prior publications.[40 41] In preliminary experiments where indicated, CD4^{+} and CD8^{+} TILs were enriched by negative or positive selection using CD8 microbeads, respectively (Miltenyi Biotec, Gaithersburg, Maryland, USA). Additionally, the IFNg Secretion Assay—Detection Kit (PE) (Miltenyi Biotec) in combination with anti-PE MicroBeads (Miltenyi Biotec) was used for positive selection of IFNg-producing CD4^{+} TIL, following the manufacturer's protocol only where indicated. See online supplemental figure 1 for representative enrichment by flow cytometry.

DNA/RNA extraction for neoantigen detection
Additional excess tumor tissue was preserved as formalin-fixed, paraffin-embedded (FFPE) or snap frozen (SF) tumor blocks within 15 min of surgical extirpation. FFPE tissues were placed in 10% neutral buffered formalin and fixed for 24 hours prior to embedding in paraffin using standard methodologies. SF tissues were immediately frozen and stored in liquid nitrogen until processing. Sections (4 uM) from each tumor block were stained with H&E and reviewed by the study pathologist to ensure tumor content. DNA and RNA from patient 1 were extracted with the QIAamp DNA FFPE Tissue Kit (Qiagen Sciences, Germantown, Maryland, USA) and Ambion RecoverAll Kit (ThermoFisher Scientific), respectively. RNA for this patient was DNase treated, followed by cleanup with the RNeasy MinElute Cleanup Kit (Qiagen Sciences). For all other patients, DNA and RNA were extracted with the Allprep DNA/RNA kit (Qiagen Sciences). Genetic material was quantified by Qubit fluorometric quantification (ThermoFisher Scientific, Waltham, Massachusetts, USA) and quality control (QC) was performed using the TapeStation 4200 System (Agilent Technologies, Santa Clara, California, USA).

Whole-exome sequencing/RNA-sequencing
Patient 1
Whole-exome sequencing (WES) was performed on DNA from fixed tumor tissue (FFPE) and from blood as a germline control in order to identify somatic mutations in the coding regions of the human genome. Following a quantitative-PCR (qPCR)-based DNA quality and quantity assessment using the Agilent NGS FFPE QC Kit with the tumor DNA sample, 200 ng of DNA was used as input into the Agilent SureSelect XT Clinical Research Exome kit (Agilent Technologies). Briefly, for each tumor DNA sample, a genomic DNA library was constructed according to the manufacturer's protocol and the size and quality of the library was evaluated using the Agilent BioAnalyzer. An equimolar amount of library DNA was used for a whole-exome enrichment using the Agilent capture baits and after qPCR library quantitation and QC analysis on the BioAnalyzer, approximately 200 million and 80 million 75-base paired-end sequences for the tumor and germline control sample, respectively, were

generated using v2 chemistry on an Illumina NextSeq 500 high-output sequencing run (Illumina, San Diego, California, USA).

An RNA-sequencing (RNASeq) library was prepared using the Illumina TruSeq RNA Exome Library Preparation Kit (Illumina) according to the manufacturer's protocol. Briefly, following RNA quality review on the Agilent TapeStation (Agilent Technologies) and quantitation with the Qubit RNA BR Assay Kit (ThermoFisher Scientific), 100 ng of RNA was used as input RNA fragmentation. The cDNA libraries were generated according to the protocol and reviewed for quality and quantity using the Qubit dsDNA Assay Kit and the Agilent BioAnalyzer DNA 1000 Chip (Agilent Technologies). The library was then enriched twice using the Illumina exome probes. The final library was reviewed for initial quantity and quality using the Qubit dsDNA Assay Kit (ThermoFisher Scientific) and the BioAnalyzer High Sensitivity DNA Chip (Agilent Technologies). Following library quantitation with the Kapa Library Quantification Kit for NGS (Roche Sequencing, Pleasanton, California, USA), the library was sequenced on an Illumina NextSeq 500 (Illumina) mid-output run to generate 174 M million pairs of 75-base reads.

For confirmation of the expression of the $S100A11^{Q22R}$ mutation in the FFPE tumor tissue from patient 1, RNA was extracted and DNase treated prior to processing with the Nugen RNASeq Universal Kit (Tecan US, Morrisville, North Carolina, USA). The generated cDNA was quantified and reviewed for QC metrics, then sequenced on the NextSeq 500 (Illumina) 2×75 base pair mid-output run and analyzed for nucleic acid conversion (T>C) at position Chr1 152 006 215 in the human genome version hs37d5.

Patient 2
WES was performed on DNA from frozen tumor tissue and from blood as a germline control in order to identify somatic mutations in the coding regions of the human genome. Briefly, 200 ng of DNA was used as input into the Agilent SureSelect XT Clinical Research Exome kit (Agilent Technologies). For each tumor DNA sample, a genomic DNA library was constructed according to the manufacturer's protocol and the size and quality of the library was evaluated using the Agilent BioAnalyzer. An equimolar amount of library DNA was used for a whole-exome enrichment using the Agilent capture baits and after qPCR library quantitation and QC analysis on the BioAnalyzer. Approximately 195 million and 134 million 75-base paired-end sequences for the tumor and germline control sample, respectively, were generated using v2 chemistry on an Illumina NextSeq 500 high-output sequencing run (Illumina).

An RNAseq library was prepared using the NuGen FFPE RNA-Seq Multiplex System (later renamed to Universal RNA-Seq Library Preparation Kit with NuQuant, (Tecan US,). DNase-treated RNA (100 ng) was used to generate cDNA and a strand-specific library

following the manufacturer's protocol. Library molecules containing ribosomal RNA sequences were depleted using the NuGen AnyDeplete probe-based enzymatic process. The final library was assessed for quality on the Agilent TapeStation (Agilent Technologies, Wilmington DE), and quantitative RT-PCR for library quantification was performed using the Kapa Library Quantification Kit (Roche Sequencing). The library was sequenced on an Illumina NextSeq 500 mid-output sequencing run to generate 125 million pairs of 75-base reads.

Patients 3–6
WES was performed on DNA from frozen tumor tissues and from blood as germline controls in order to identify somatic mutations in the coding regions of the human genome. Briefly, 200 ng of DNA was used as input into the Agilent SureSelect XT Clinical Research Exome kit (Agilent Technologies). For each tumor DNA sample, a genomic DNA library was constructed according to the manufacturer's protocol and the size and quality of the library was evaluated using the Agilent BioAnalyzer. An equimolar amount of library DNA was used for a whole-exome enrichment using the Agilent capture baits and after qPCR library quantitation and QC analysis on the BioAnalyzer, approximately 110 million and 60 million 75-base paired-end sequences for the tumor and germline control samples, respectively, were generated using V.2 chemistry on an Illumina NextSeq 500 high-output sequencing run (Illumina).

An RNAseq library was prepared using the Universal RNA-Seq Library Preparation Kit with NuQuant, (Tecan US). Briefly, 100 ng of DNase-treated RNA was used to generate cDNA and a strand-specific library following the manufacturer's protocol. Library molecules containing ribosomal RNA sequences were depleted using the NuGen AnyDeplete probe-based enzymatic process. The final library was assessed for quality on the Agilent TapeStation (Agilent Technologies), and quantitative RT-PCR for library quantification was performed using the Kapa Library Quantification Kit (Roche Sequencing). The library was sequenced on an Illumina NextSeq 500 mid-output sequencing run to generate >80 million pairs of 75-base reads per sample.

Neoantigen peptide detection and MHC binding analysis
WES data from matched tumor and germline specimens were aligned to human genome version hs37d5 with the Burrows Wheeler Aligner (BWA) algorithm (V.0.5.9-r16) and refined with Picard (V.1.56, http://picard.sourceforge.net/) and the Genome Analysis Toolkit (GATK2Lite-2.2).[42 43] Somatic point mutations were detected with MuTect (V.1.14), SomaticIndelDetector (via GATK2Lite), and Strelka (V.1.0.13) (Illumina) analysis tools and annotated with ANNOVAR software.[44–46] Somatic mutations observed as passing in Strelka, or passing in MuTect and observed at all in Strelka were used to predict altered peptides from the ANNOVAR results. RNA sequencing (RNASeq) data from tumor specimens

were aligned via the Spliced Transcripts Alignment to a Reference (STAR, V.2.5.3a) algorithm and quantitated by the High-Throughput Sequence Analysis tool (V.0.6.0) (HTSeq) to confirm gene expression and verify mutation identification.[47 48]

Each patient's complete HLA haplotype was predicted by RNASeq analysis via the Optitype (HLA-I, V.1.3.2) and PHLAT (HLA_II, V.1.1) algorithms.[49 50] This HLA profile was used to predict the binding of the mutated peptides to MHC class I and MHC class II components by netMHCpan (V.4.0) and netMHCIIpan (V.3.2), respectively.[51 52] Mutant and wildtype peptides were extracted from the ANNOVAR output and binding peptide sizes of 8–14 amino acids (MHC-I) and 12–16 amino acids (MHC-II) were tested.

Neoantigen peptide prioritization

Mutated peptides were prioritized based on expression and MHC binding prediction analyses to obtain an Additive Score (AS). The expression score (ES) component was determined using the maximum variant allele frequency in the RNAseq data (VAF) and fragments per kilobase of exon per million mapped fragments (FPKM) from the RNASeq data. The MHC combined score (MCS) component added the maximum predicted binding of each peptide to the patient's MHC molecules and the Differential Agretopicity Index (DAI) between the variant (var) peptide and its corresponding reference (ref) peptide for MHC class I (mhc1) and MHC class II (mhc2). The full AS formula for prioritizing 25-mers is below:

$AS = ES + (MCS/1.5)$.

$ES = max\_VAF\_RNA\_percentile + (0.5 \times max\_FPKM\_percentile)$.

$MCS = mhc1\_score + (0.5 \times \$mhc2\_score)$.

$mhc1\_score = ic50\_mhc1\_percentile + (0.5 \times DAI\_mhc1\_percentile)$.

$mhc2\_score = ic50\_mhc2\_percentile + (0.5 \times DAI\_mhc2\_percentile)$.

percentile = max percentile for a given peptide within 25-mer (excluding 0/NA).

$DAI: var\_ic50/ref\_ic50$.

Custom peptide synthesis

Prioritized peptides were synthesized individually as 25mers using the PEPotec Immuno Custom Library (ThermoFisher Scientific) and Custom Peptide Synthesis (JPT Peptide Technologies, Berlin, Germany) platforms or as a peptide pool (PP) via the PepMix Peptide Pools platform (JPT Peptide Technologies). For patient 1, an additional custom library of overlapping 12-16mer peptides harboring the S100A11^{Q22R} mutation were synthesized as well as the wildtype 25mer (WT; S100A11^{WT}) via the PEPotec Immuno Custom Peptide Library platform (ThermoFisher Scientific). All peptides were reconstituted in dimethyl sulfoxide (DMSO) and used at the indicated concentrations.

APC generation

Autologous dendritic cells (DCs) were derived from cryopreserved mononuclear cells from patient apheresis specimens collected as part of the clinical protocol prior to preconditioning lymphodepletion. Cells were cryopreserved in 90% human serum supplemented with 10% DMSO initially using the Mr. Frosty Freezing Container system (ThermoFisher Scientific) according to the manufacturer's protocol prior to transfer to long-term storage in vapor phase liquid nitrogen cryounits (ThermoFisher Scientific). Briefly, cells were thawed in warm RPMI-based media containing 10% human Ab serum (Lot 20800: Omega Scientific, Tarzana, California, USA; Lot H16Y00K: Gemini Bio Products, West Sacramento, California, USA; Lot A14006: Access Biologicals, Vista, California, USA) and 6.7 µg/mL DNase I (MilliporeSigma, St. Louis, Missouri, USA). Human serum was pretested for suitability in TIL cryopreservation, generation and expansion, functional assays, as well as sterility measures prior to use. All cells were plated at 37°C at a concentration of 1×10^7/mL in DC Media (CellGenix, Portsmouth, New Hampshire, USA). All non-adherent cells and media were removed after 90 min and replaced with fresh DC Media supplemented with 100 ng/mL GM-CSF (R&D Systems, Minneapolis, Minnesota, USA) and 20 ng/mL IL-4 (Miltenyi Biotec). Three days later, an equivalent volume of this same media was added. On day 5, DC Media was removed and DC were washed with warm PBS and collected in warm PBS-EDTA (Lonza Group AG, Basel, Switzerland) using a cell scraper to detach adherent cells.

Autologous B cells were transformed from peripheral blood lymphocytes (PBL) using Epstein-Barr Virus (EBV) supernatants produced by the B95-8 cell line (a kind gift from Dr. Ken Wright, MCC), according to established protocols.[53] Briefly, 1×10^7 PBL were added to an upright T25 flask in 5 mL of tumor complete media (TCM), 5 mL of EBV supernatant, and 0.5 µg/mL of ciclosporin A (ThermoFisher Scientific). TCM consisted of RPMI containing 10% fetal bovine serum (FBS; Atlanta Biologicals, Flowery Branch, Georgia, USA). B cells were incubated until macroscopic clusters were observed and propagated until sufficient numbers were generated for downstream applications. Flow cytometric analysis was used to confirm population purity and expression of canonical B cell markers CD19 and CD20 (panel below).

TIL neoantigen peptide stimulation

Autologous APCs were cultured at 3.6×10^6/well in six-well plates and loaded with the complete pool of patient-specific mutant 25mer peptides (2.5–100 ng/mL each) at equal concentrations for approximately 24 hours in DC Media (CellGenix). APCs were washed three times in PBS to remove unbound peptide and replated in six-well plate format for the coculture. TIL, rested overnight in RPMI supplemented with 10% human Ab serum (TIL CM) and 3000 IU/mL recombinant human (rh) IL-2 (aldesleukin, a generous gift from Prometheus Laboratories, San Diego, California, USA), were enumerated

and added to the peptide-loaded APCs at a 1:1 ratio for overnight coculture. Coculture media was supplemented with 300 IU/mL rhIL-2 to promote TIL viability. Cells were collected and stained for fluorescence-activated cell sorting (FACS) under sterile conditions according to the below procedure. Cell culture supernatants were assayed individually for IFNg by the Single Plex immunoassay or simultaneously for IFNg, TNFa, and Granzyme B using the multianalyte immunoassay and analyzed on the Ella machine (Protein Simple, San Jose, California, USA).

Fluorescence-activated cell sorting

All cells were collected and washed in sterile PBS, then stained with the Live/Dead Fixable Near-IR Dead Cell Stain Kit (ThermoFisher Scientific) according to the manufacturer's protocol at 1×10^7 cells/mL. Cells were then washed with sterile Flow Cytometry Buffer (FCB) and stained with surface antibodies. FCB consisted of 5% FBS, 1 mM EDTA, and 0.1% sodium azide in PBS. Anti-human cell surface antibodies were added according to the following panel: CD11c BV650 (clone B-ly6; BD Biosciences, San Jose, California, USA), CD3 BV785 (clone UCHT; BioLegend, San Diego, California, USA), CD4 FITC (clone RPA-T4; BD Biosciences), CD8 BV510 (clone SK1; BioLegend), CD134 (OX40) BV421 (clone BerACT-35; BioLegend), CD137 (4-1BB) PerCyCy5.5 (clone 4B4-1; BioLegend). B cells were used as APCs when DCs were unavailable. In this event, CD20 BV650 (BD Biosciences) replaced CD11c BV650 in the sort staining panel. Cells were stained at 4°C for 20 min, then washed with sterile FCB and resuspended in Complete OpTmizer Media for FACS. Complete OpTmizer Media consisted of CTS™ OpTmizer T cell Expansion SFM (no phenol red; ThermoFisher Scientific) supplemented with CTS Immune cell SR (ThermoFisher Scientific), GlutaMAX Supplement (ThermoFisher Scientific) and 300 IU/mL rhIL-2. TIL were sorted at a concentration of 5×10^6–1×10^7 cells/mL in Complete OpTmizer Media.

Neoantigen-specific TILs were sorted on a BD FACSAria SORP (BD BioSciences) for increased cell surface expression of 4-1BB and OX40 between peptide-stimulated TIL and unloaded controls. Additional control wells were set up in a 96-well format with 1×10^5 TIL to assist with gating: (1) fluorescence minus one (FMO) staining for 4-1BB on TIL cocultured with 1×10^5 peptide-loaded APCs; (2) FMO for OX40 on TIL cocultured with 1×10^5 peptide-loaded APCs; (3) Dynabeads human T-activator CD3/CD28 (ThermoFisher Scientific) at a 1:1 TIL:bead ratio; (4) TIL cultured without APCs in media only. TIL activated by neoantigen peptides upregulated either 4-1BB or OX40 and were sorted as 'positive' while TIL that did not increase expression of either marker were sorted as 'negative.' TILs were sorted directly into human Ab serum supplemented with gentamicin, then washed twice with TIL CM. TIL were expanded via REP prior to validation and downstream experiments.

MHC class II expression

AT was induced to express MHC class II by (1) pretreatment with recombinant human (rh) IFNg (ATg) or (2) transduction with the class II Transactivator (AT-CIITA). (1) Recombinant human IFNg (500 U/mL; R&D Systems) was added to TCM and cells were cultured for 5–7 days total, with media replacement on day 3. (2) AT was transduced using CIITA viral supernatant supplemented with 4 µg/mL polybrene (Sigma-Aldrich, St. Louis, Missouri, USA). Tumor cells were centrifuged with viral supernatant at 800 relative centrifugal force (rcf) for 90 min at 37°C, then expanded in TCM prior to puromycin (1 µg/mL; Sigma-Aldrich) selection. MHC class II expression was confirmed by flow cytometry.

TIL coculture

Effector (E) and target (T) cells were cocultured at a 1:1 E:T ratio in a 96-well plate format with 1×10^5 cells each (counted by hemacytometer). Effector cells consisted of TIL or TCR-T (below). Target cells consisted of AT, HLA-matched tumor, or EBV-transformed B cells. AT was enforced to express MHC class II where indicated as described above. Target cells were loaded with individual peptides or a pool of peptides (2.5–150 ng/mL each) overnight prior to coculture. Blocking antibodies were added 1 hour prior to coculture initiation in order to precoat target cells and remained in the assay well for its duration at a final concentration of 10 µg/mL. Anti-human blocking antibodies used: HLA-ABC (clone W6/32; BioLegend), HLA-DR, DP, DQ (clone Tü39; BioLegend), HLA-DR (clone L243; BioLegend), HLA-DP (clone B7/21; Leinco Technologies, Fenton, Missouri, USA), HLA-DQ (clone SPV-L3; Novus Biologicals, Littleton, Colorado, USA). Cell culture supernatants were collected and IFNg production was quantified by IFNg ELISA (R&D Systems) or the Ella system (described above).

Flow cytometry

Following coculture in a U-bottom 96-well plate format, TIL were transferred to a V-bottom 96-well plate, washed with PBS and stained with Live/Dead Fixable Near-IR Dead Cell Stain Kit (ThermoFisher Scientific) according to the manufacturer's protocol. TIL were then washed with FCB and stained with cell surface antibodies for 30 min at 4°C, protected from light. Cells were washed with FCB and fixed. For surface staining, TIL were fixed in 2% paraformaldehyde (PFA) until acquisition.

For intracellular cytokine staining, GolgiStop and GolgiPlug (BD Biosciences) were added at ×0.5 according to the manufacturer's recommended dosage at the initiation of coculture. For degranulation potential, CD107a (LAMP-1) BV785 (clone H4A3; BioLegend) was also added at coculture initiation.[41] TIL were viability and surface stained as above, then processed and stained with the Fixation/Permeabilization Solution Kit (BD Biosciences) according to the manufacturer's protocol and fixed in 2% PFA until data acquisition. Data acquisition

was performed on a BD Celesta or BD LSRII (BD Biosciences) and analyzed with FlowJo Software (TreeStar, Ashland, Oregon, USA).

Flow cytometry antibodies

The following anti-human antibodies were used for flow cytometry as described above: CD3 BV785 (clone UCHT1; BioLegend.), CD4 FITC (clone RPA-T4; BD Biosciences), CD8 BV510 (clone SK1; BioLegend.), CD11c BV650 (clone B-ly6; BD Biosciences), CD20 BV650 (clone 2H7; BD Biosciences), CD25 PECy7 (clone M-A251; BD Biosciences), CD39 BV605 (clone A1; BioLegend.), CD69 BV510 (clone FN50; BioLegend), CD107a (LAMP-1) BV785 (clone H4A3; BioLegend), CD127 APC (clone A019D5; BioLegend.), CD134 (OX40) BV421 (clone BerACT35; BioLegend.), CD137 (4-1BB) PerCpCy5.5 (clone 4B4-1; BioLegend), CD183 (CXCR3) BV421 (clone 1C6; BD Biosciences), CD223 (LAG-3) BV650 (clone 11C3C65; BioLegend), CD279 (PD-1) BV785 (clone EH12.2H7; BioLegend), CD366 (TIM3) APC (clone F38-2E2; eBiosciences), BTLA BV650 (clone J168-540; BD Biosciences), Granzyme B PacBlue (clone GB11; BioLegend), IFNg APC (clone 4S.B3; eBiosciences), TNFa PECy7 (clone Mab11; eBiosciences).

Infused TIL products used in clinical trial protocols were cell surface stained and analyzed as previously described to determine CD4 and CD8 frequency in the TIL product.[2 8 54]

TCRβ sequencing

DNA was extracted from TIL and PBMC via the DNeasy Blood and Tissue Kit or AllPrep DNA/RNA Mini Kit (Qiagen Sciences) and quantified by Nanodrop (ThermoFisher Scientific). When necessary, DNA was precipitated using isopropanol and re-quantified. DNA was analyzed using the ImmunoSeq TCRb Kit V.3 and V.4 (Adaptive Biotechnologies, Seattle, Washington, USA) at the MCC Molecular Genomics Core or the Adaptive Biotechnologies ImmunoSeq Laboratory. Data were uploaded to the Adaptive ImmunoSEQ Analyzer V.3.0 for analysis of shared TCRb CDR3 amino acid sequences.

Incucyte live cell imaging

Autologous EBV-transformed B cells (targets) were pulsed with 100–150 ng/mL of peptide overnight. Target cells were labeled with 0.2 uM Incucyte Cytolight Rapid Green Dye (Essen Bioscience, Ann Arbor, Michigan, USA) according to the manufacturer's protocol, washed, and plated in Complete OpTmizer Media at 2×10^4 Target cells/well in a flat bottom 96-well plate. The assay plate was precoated with poly-L-ornithine (Sigma-Aldrich) for 60 min at room temperature, then allowed to air dry for 30 min at room temperature. Peptides (100–150 ng/mL) and IL-2 (300 IU/mL) were included for the duration of the assay. The Incucyte Caspase 3/7 Red Dye (Essen Biosciences) was resuspended in Complete OpTmizer Media and added to each well at a final concentration of 2 uM/well. TIL (effectors) were rested overnight in

TIL CM supplemented with 3000 IU/mL rhIL-2, then counted by hemacytometer, and added to the assay plate at 1:1, 2.5:1, 5:1, and 10:1 E:T ratios. Coculture plates were immediately placed in the Incucyte S3 Live Cell Analysis Instrument (Essen Biosciences) and images were acquired at 30 min intervals for 6 hours. Data analysis was completed with the Incucyte S3 Software V.2018B (Essen Biosciences) and exported to GraphPad Prism V.9 (GraphPad Software, La Jolla, California, USA).

Real-time cell analysis immune cell killing assay

AT cell targets were collected with 0.05% trypsin (ThermoFisher Scientific), enumerated, and plated on the E-Plate 96 PET (Agilent Technologies) in TIL CM at a concentration of 1×10^5 cells/well. Each AT-bearing plate was initially calibrated on the xCELLigence real-time cell analysis (RTCA) MP instrument (Agilent Technologies), then incubated for approximately 24 hours within the analyzer chamber. Enriched TIL (effectors) were added to the plate at 1:1, 2.5:1, 5:1, and 10:1 E:T ratios in triplicate and returned to the RTCA analyzer chamber for 6 hours. Plate sweeps occurred at 15 min intervals and measured cellular impedance of AT in real-time during each step. Maximum target cell death was achieved via addition of 2% Triton X-100 (MilliporeSigma) in lieu of effector cells. Data were acquired and analyzed with the RTCA Software Pro Immunotherapy Module (Agilent Technologies) and exported for analysis and visualization with GraphPad Prism v9 (GraphPad Software) for data visualization.

Transgenic T Cell Receptor-Engineered T Cell (TCR-T) production

Full-length T cell receptor (TCR) alpha and beta chain sequences were extracted from scRNASeq VDJ analysis and synthesized as double-stranded DNA fragments (gBlock; Integrated DNA Technologies, Coralville, Iowa, USA). The TCR sequences were arranged in tandem, linked by the porcine teschovirus-1 (P2A) self-cleaving peptide sequence, and flanked by restriction enzyme sites (NcoI and NotI) to create the insert sequence. The insert and plasmid backbone (MSGV1) were digested, purified, and ligated.[55] The full TCR plasmid was transformed into One Shot Stbl3 chemically competent *Escherichia coli* (ThermoFisher Scientific) and amplified on LB agar plates containing ampicillin (100 μg/mL) for purification by the QIAGEN Plasmid Maxi Kit (Qiagen Sciences) according to the manufacturer's protocol. The TCR plasmid and envelope protein plasmid (RD114) were cotransfected into 293GP cells using Lipofectamine 2000 (ThermoFisher Scientific) as previously described.[55] Retroviral supernatants were collected at 48, 72, and 96-hours following transfection, filtered at 0.45 microns, and used for TCR-T transduction.

Allogeneic PBLs were isolated from whole blood via Ficoll-Hypaque density gradient (MP Biomedicals, Santa Ana, California, USA) and red blood cells lysed with ACK lysis buffer (ThermoFisher Scientific). T cells were

activated with 0.25 µg/mL of anti-CD3 (clone: OKT3; BioLegend) for 48 hours in X-VIVO media (Lonza Group AG) supplemented with 5% HS (Gemini Bio-Products, Sacramento, California, USA), 1% L-glutamine (ThermoFisher Scientific), and 300 IU/mL IL-2 (Proleukin, Clinigen Group, Burton upon Trent, UK). Six-well plates were precoated with 20 µg/mL RetroNectin (Takara Bio, Kusatsu, Shiga, Japan), then blocked with PBS supplemented with 2% bovine serum albumin (MilliporeSigma). After rinsing with PBS, 2 mL of viral supernatant was added to the RetroNectin-coated plates with an equal volume of DMEM supplemented with 10% FBS. Plates were centrifuged at 2000 rcf for 2 hours at 32°C. Activated αβ T cells were transferred to viral-coated plates at 2e6 T cells/well and centrifuged for ten minutes at 1000 rcf at 32°C, then incubated at 37°C overnight. This transduction procedure was repeated after 24 hours in a duplicate set of precoated six-well plates as above. Following transduction, the TCR-T cells were transferred to flasks and expanded for 72 hours in X-VIVO media supplemented with 300 IU/mL IL-2. TCR-T cells were evaluated for transduction efficiency by flow cytometric detection of the mTCRb construct (anti-mouse TCRbeta PerCP/Cy5.5, clone H57-597; BioLegend) on viable CD4$^+$ (anti-human CD4 PECy7, clone RPA-T4; BioLegend) and CD8$^+$ lymphocytes (anti-human CD8 BUV395 RPA-T8; BD Biosciences) and used in functional assays.

Single cell RNA sequencing

Sorted TIL from six melanoma patients were cryopreserved (as above) following REP and scRNASeq was performed by Turnstone Biologics immediately on thaw. TIL were counted via the Countess Automated Cell Counter (ThermoFisher Scientific) with trypan blue, filtered, and resuspended between 700 and 1300 cells/µL in order to sequence 2000 cells per sample. The Chromium Next GEM Single Cell 5' Reagent Kits V.2 (Dual Index) (10x Genomics, Pleasanton, California, USA) was used for paired TCR and scRNA sequencing following the manufacturer's protocol. The Chromium Next GEM Chip K was loaded with gel beads in emulsion (GEM) containing T cells, master mix components, barcoded gel beads, and partitioning oil. Reverse transcription generated barcoded cDNA and V(D)J sequences for amplification, followed by 5' Gene Expression (GEX) and V(D)J library construction. Sequencing was performed on the NextSeq 1000 Instrument (Illumina) at a depth of 60 million (GEX) and 30 million (V(D)J) paired-end reads, per sample.

Single-Cell RNA-Seq data processing, filtering, batch effect correction, and clustering

Raw sequencing reads for each sample were processed using Cell Ranger (V.6.1, 10X Genomics) and aligned against GRCh38 human transcriptome. Barcodes with unique molecular identifier (UMI) counts passing threshold were imported to Seurat V.4.2.0 for further analysis.[56] Genes detected in less than 3 cells were excluded; cells with less than 200 genes detected or greater than 10% mitochondrial UMIs were filtered out. Doublets were detected using Scrublet, DoubletFinder, scDblFinder, and doubletCells implemented in scran, assuming 0.08% doublet rate for every 1000 sequenced cells.[57–60] Cells identified as doublets by at least two algorithms were removed from further analysis. UMI counts were log normalized. The top 5000 variable genes were identified using FindVaribleFeatures function with 'vst' method. T cell receptor and immunoglobulin genes were removed from the variable genes to prevent clustering based on V(D)J transcripts. S and G2/M cell cycle phase scores were assigned to cells using CellCycleScoring function. Top 40 principal components were generated by RunPCA and further used to construct the uniform manifold approximation and projection (UMAP) by RunUMAP. Clusters were identified by Louvain algorithm using *FindCluster* at resolution=1. For each sample, the CD8$^+$ and CD4$^+$ T cells were identified based on expression of *CD3E, CD3D, CD4, CD8A*, and *CD8B*, as well as clustering results as following: (1) CD4$^+$*CD8A*$^-$CD8B$^-$ cells were assigned as CD4$^+$ cells; (2) *CD4$^-$CD8A$^+$*/CD8B$^+$ cells were assigned as CD8$^+$ cells; 3) For CD4$^+$*CD8A$^+$*/CD8B$^+$ cells, the cells with log2(*CD4/CD8*) >1 and clustered with CD4$^+$ cells were assigned as CD4$^+$, while the cells with log2(*CD4/CD8*) <1 and clustered with CD8$^+$ cells were assigned as CD8$^+$.

The CD4$^+$ cells from individual samples were further integrated to remove batch effects using FindIntegrationAnchors and IntegrateData functions with 8000 anchor genes and 40 dimensions of canonical correlation analysis.[61] Integrated data were regressed against total UMIs, percentage (%) of mitochondrial UMIs, and cell cycle phase scores using ScaleData. A shared nearest neighbor based graph was constructed using top 40 principal components, and clusters were identified by Louvain algorithm using FindCluster at resolution=1. UMAP projections were generated by RunUMAP and used for all visualizations.

Differential gene expression analysis and cluster annotation

Differential expression analysis comparing each cluster vs all others was performed using FindAllMarkers function in Seurat with default settings. Genes with log2(foldchange)>0.25 and Bonferroni-corrected p value<0.05 were considered differentially expressed. Clusters were annotated by comparing differential genes to markers reported in previous scRNA-seq studies.[62–65] Clusters were merged into cell types based on above annotation. Enrichment scores of the T cell exhaustion gene set (*TOX, LAG3, PDCD1, HAVCR2, ITGAE, TIGIT, CXCL13*) and the T cell stemness gene set (*TCF7, CDCR5, CD28, GZMK, CCR7, IL7R, BCL6, SELL*, CD27) were calculated using *AUCell* algorithm implemented in SCENIC.[66] Cells localized to the 'proliferative' cluster were present across all patient samples and excluded from the analysis in order to focus the analysis on transcriptional programs related to neoantigen specificity rather than non-specific

signals received during REP. Marker genes expression was visualized on the UMAP or by violin plot using log-normalized UMI counts. A bubble plot was used to visualize z-score normalized average expression of genes previously reported in neoantigen-specific T cell signatures and percentage of expressing cells per cluster or per cell type.[34–39] Expression distribution of marker genes were compared between cell types using Violin plots.

Gene Set Enrichment Analysis

Differential expression analysis was performed comparing cells within each cell type vs all other cells, followed by a gene set enrichment analysis (GSEA). For each cell type, genes were ranked based on −log10(p value)×(-sign of log2(fold-change)) resulted from the differential analysis, with the most upregulated genes at top and the most downregulated genes at bottom. Preranked GSEA was performed on gene rankings using R package fgsea with 10,000 permutations, against Hallmarks, KEGG, BIOCARTA, REACTOME, PID, Gene Ontology, and ImmuneSigDB databases from MsigDB.[67–71] The normalized enrichment scores (NESs) were visualized using GraphPad Prism for selected pathways. Full GSEA is reported in the online supplemental data.

Single-Cell 10X V(D)J analysis

TCR reads sequenced by 10X V(D)J assay were aligned to human GRCh38 reference transcriptome using Cell Ranger VDJ (V.6.1, 10X Genomics) to assemble the single TCR chains. Only the assembled chains that were highly confident, of full-length, and productive were kept for downstream analysis. Cells with the same amino acid sequences of the CDR3 regions and V(D)J genes for both TRA and TRB chains were considered originated from the same clone. These cells were further assigned to cell types based on their annotation of the paired single-cell RNA assay. Identified TCRs were matched to the known sequences of neoantigen specific TCRs in each patient. Cells expressing neoantigen specific TCRs were visualized on UMAP projected generated from paired RNA assay.

General lab operation

These studies were completed in research laboratories and core facilities at MCC and in collaboration with Turnstone Biologics. TILs generated for clinical use were produced under Good Manufacturing Practices conditions, as previously reported.[2 8 54] Assays were completed using established and investigative protocols as described here for general research purposes and validated as outlined.

Statistics

All statistical analyses used GraphPad Prism V.9 (GraphPad Software) with statistical methods reported in figure legends. Unless otherwise indicated, error bars represent mean and SD of technical replicates.

Patient samples were collected under the clinical trial protocols NCT01005745 (patients 1, 2, 5), NCT01701674 (patient 3), and NCT01659151 (patients 4 and 6).[2 8 54]

RESULTS
Patient 1

Patient 1 presented with M1c metastatic melanoma refractory to multiple treatments prior to ACT using TIL. Surgical resection of an intramuscular arm lesion yielded 48 fragments for TIL generation, resulting in 5.2×10^{10} predominantly CD4$^+$ TIL (88%) for infusion 101 days following surgery.[2] Multiple metastases were quickly resolved on ACT, and the patient ultimately achieved an ongoing long-term CR of greater than 10 years (figure 1A,B). Infused TIL failed to produce IFNg in vitro in response to autologous tumor (AT). As the infusion product contained a low proportion of CD8$^+$ T cells, we hypothesized that enriching this fraction would uncover tumor specificity given the observed tumor regression following TIL transfer. However, coculture with a panel of HLA-matched melanoma tumors still did not elicit IFNg release by the CD8$^+$ TIL (online supplemental figure 1A–C). As standard methods for tumor reactivity by CD8$^+$ T cells did not seem to reflect the overwhelming clinical response, we posited that neoantigen recognition by CD4$^+$ T cells could be driving the antitumor response in vivo.

To investigate this, we performed whole exome (WES) and RNA sequencing (RNASeq) from surgical tumor tissue in order to determine this patient's neoantigen repertoire. In total, 91 non-synonymous mutations were detected and 79 of these mutations were scored by expression level and predicted binding affinity to the patient's specific MHC haplotype (figure 1C). Of these, 65 peptides were amenable to custom synthesis. When pooled and loaded onto autologous DCs, efficient stimulation of the TIL infusion product was detected via upregulation of OX40 and 4-1BB, markers of antigen-specific T cell activation.[15 72] This response was confined to the CD4$^+$ TIL fraction, with minimal stimulation of the CD8$^+$ T cells (figure 1D). Further evaluation indicated that the neoantigen PP elicited a multifaceted effector response from these TIL, with the release of the cytolytic enzyme granzyme B, and the critical antitumor cytokines, IFNg and TNFa (figure 1E).

To determine precisely which neoantigens were driving the observed reactivity, we pulsed each mutated peptide individually onto APCs, followed by coculture with the infused TIL product. Only one of the 65 peptides (peptide 60, P60) produced significant signal from the TIL product in terms of costimulatory molecule induction and cytokine secretion. Again, this reactivity was produced exclusively by the CD4$^+$ TIL compartment (figure 1F). Moreover, the complement of effector molecules released in response to P60 recapitulated the response to the pooled peptides (figure 1G). Peptide 60 was identified as a mutated variant of the S100A11 protein, which carried a Q22R amino acid conversion derived from a non-synonymous T>C substitution. WES and RNASeq confirmed substantial expression of this antigen in approximately 40% of the sequenced reads from the patient's tumor tissue (online supplemental
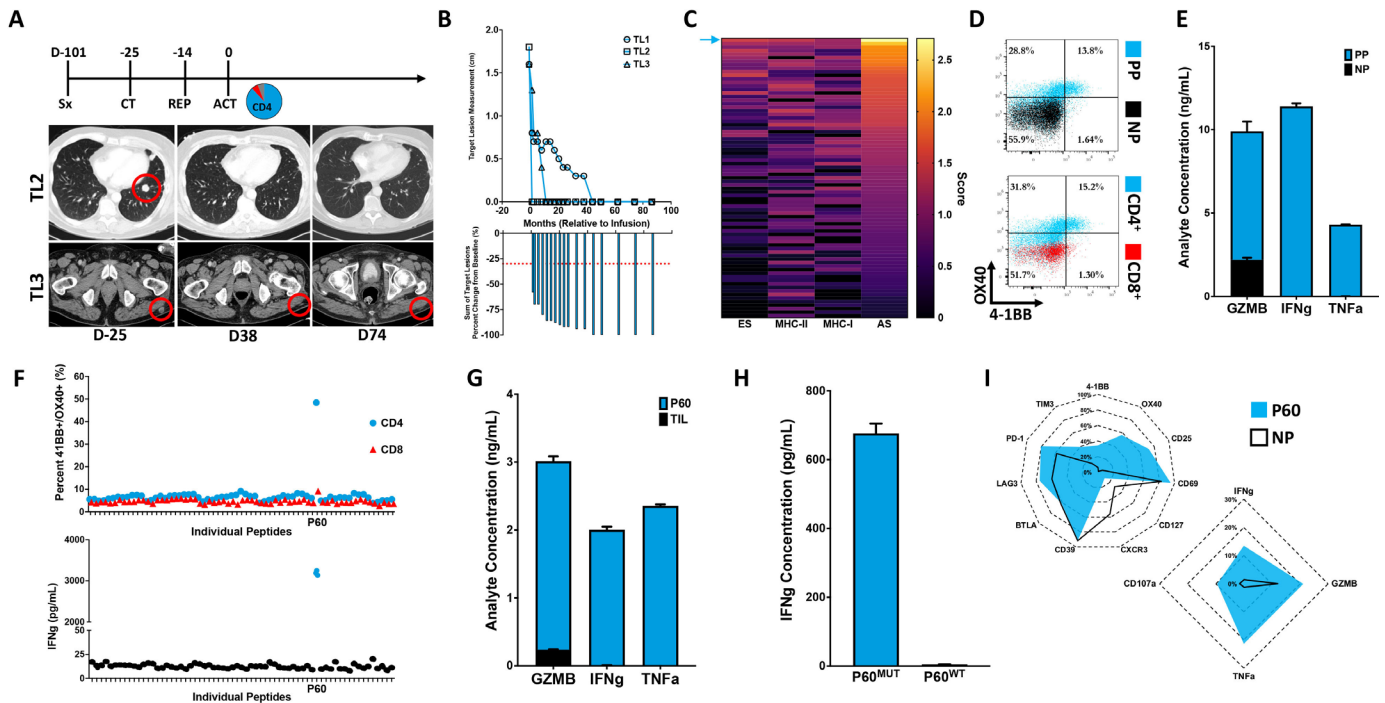
Figure 1 CD4+ TIL exhibit effector response on neoantigen peptide recognition. (A) Treatment course of ACT for patient 1, accompanied by CT images of target lesions (red circles) before and after therapy. D=day (relative to TIL infusion), Sx=surgery, TL=target lesion. (B) Measurement of the longest diameter of each target lesion (upper) and sum of target lesions (lower) during patient follow-up window. Red dotted line indicates a −30% change from the baseline sum. (C) All neoantigen peptides (n=65) were prioritized by additive score (AS). Blue arrow indicates peptide 60 (P60). See the Methods section for detailed explanation. ES=expression score, MHC-II=mhc2_ score, MHC-I=mhc1_score, (D) Bulk TILs were cocultured with DC loaded with the neoantigen peptide pool (PP) or no peptide (NP), then stained for cell sorting by OX40 and 4-1BB induction. (E) Sort coculture supernatants were assayed for TIL production of granzyme B (GZMB), IFNg, and TNFa via the Ella system. (F) TILs were validated for individual neoantigen peptide recognition by flow cytometric evaluation of OX40 and 4-1BB expression (upper) and IFNg release (lower) in coculture supernatants. (G) Enriched CD4+ TILs were assayed for effector molecule secretion in response to stimulation with P60 or no stimulation (TIL). (H) Mutant (P60^MUT=P60) and wildtype (P60^WT) versions of P60 were loaded onto APCs and used to stimulate enriched CD4+ TIL. IFNg release was quantified in coculture supernatants. (I) Following coculture of enriched TIL with P60 or NP, CD4+ TIL were stained for flow cytometric analysis of the indicated cell surface and intracellular molecules. ACT, adoptive cell therapy; APCs, antigen presenting cells; DC, dendritic cell; TIL, tumor-infiltrating lymphocyte.

figure 2A). Further, S100A11^{Q22R} ranked as the highest prioritized neoantigen from this patient (figure 1C).

We synthesized the cognate wildtype (WT) peptide to ensure that these CD4+ T cells were specific for the mutated S100A11^{Q22R} peptide. Patient 1's TIL did not produce IFNg in response to WT peptide, indicating specific recognition of the mutated version of this neoantigen (figure 1H). Further interrogation by flow cytometry revealed that the CD4+ TIL response to the S100A11^{Q22R} peptide induced upregulation of additional surface markers of activation, including LAG-3, PD-1, TIM3, CD25, and CD69, while expression of CD127 and CXCR3 were reduced. Intracellular staining revealed substantial production of Granzyme B, IFNg, TNFa, and CD107a, indicative of functional degranulation and effector cytokine production (figure 1I). Neoantigen-directed cytokine release was abrogated when target cells were precoated with either a pan-MHC Class II or HLA-DR antibody, but not with an HLA-DP or HLA-DQ antibody (figure 2A). RNA expression of the HLA-DR subunits in preserved tumor tissue supported neoantigen presentation by HLA-DR as a mechanism for antitumor

recognition by CD4+ TIL (online supplemental figure 2B). Minimal epitope screening of 12–16mer peptides spanning the full 25mer mutant peptide sequence suggested a critical recognition motif near the C-terminus (online supplemental figure 3A).

To better understand the potential impact of CD4+ TIL recognition of aberrant S100A11 expression by targets, we performed an in vitro cytotoxicity assay. Using live cell imaging, we found that CD4+ TIL rapidly clustered with target cells loaded with S100A11^{Q22R} peptide, indicating efficient recognition and interaction. Over the course of 6 hours, target cells pulsed with mutant peptide were eliminated in a dose-dependent manner, as determined by decreased target cell count and increased overlap of cleaved caspase 3/7 staining in target cells over time. These effects were not observed when targets were pulsed with WT S100A11 peptide, again demonstrating specificity of the CD4+ TIL response (figure 2B and online supplemental figure 3B).

Neoantigen-reactive TIL were enriched through FACS by upregulation of OX40 and 4-1BB (online supplemental figure 3C). A single dominant clone (>80%) with paired
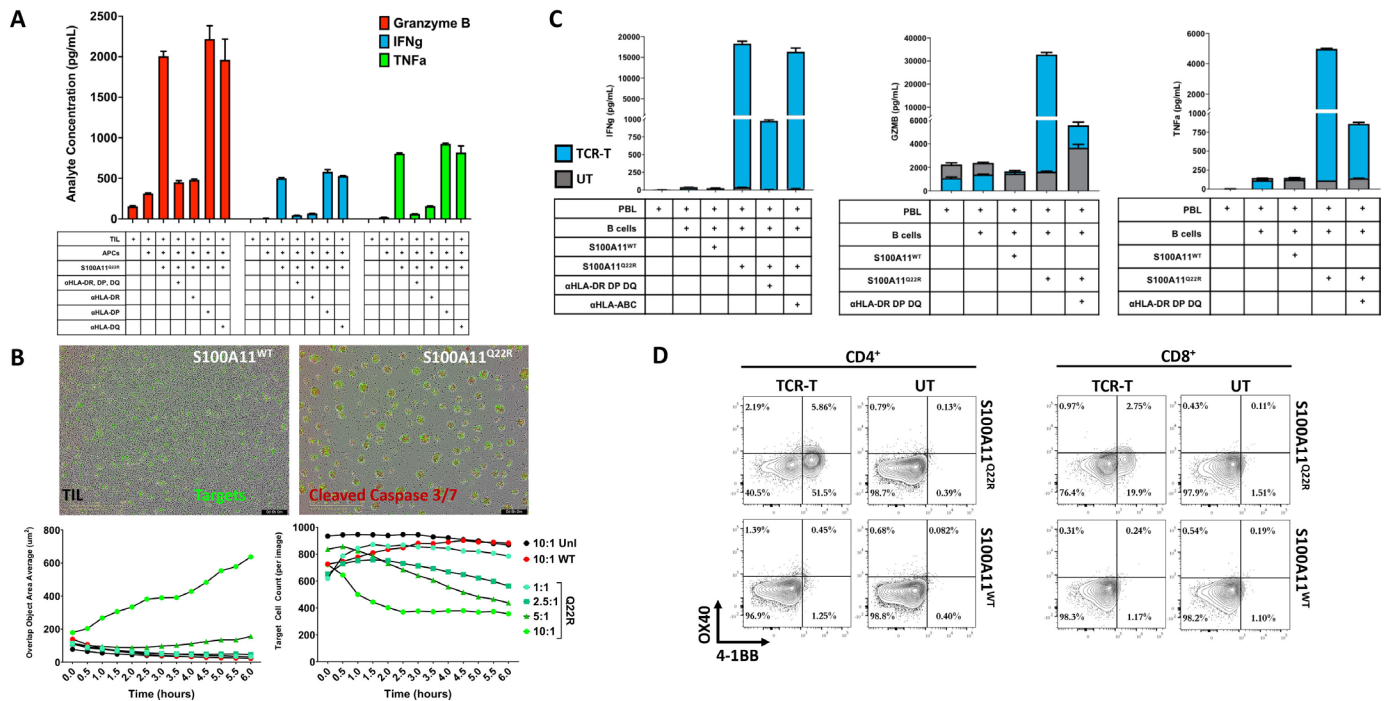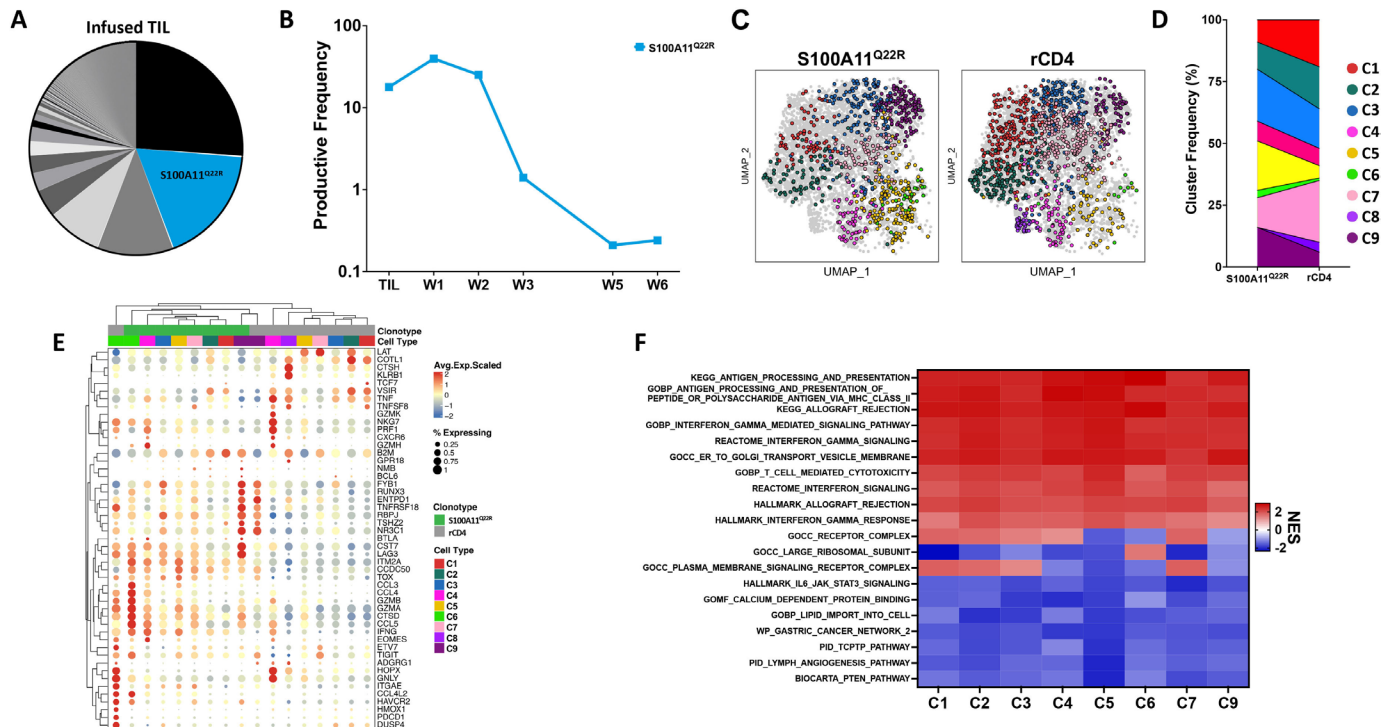
Figure 2 CD4+ TILs demonstrate cytotoxic potential restricted by TCR-HLA-DR interaction. (A) Enriched CD4+ TILs were cocultured in the indicated conditions and cell culture supernatants were analyzed for granzyme B, IFNg, and TNFa production. (B) Live cell imaging of TIL (unlabeled) and target cells (green) loaded with WT or mutated (Q22R) S100A11 peptide cocultured at indicated effector:target (E:T) ratios for 6 hours. Still image acquired at 4 hours time point with 10:1 E:T. Cleaved caspase 3/7 (red) induction was monitored via imaging at regular 30 min intervals and quantified for target cell count (bottom right) and overlap of target cells and cleaved caspase 3/7 (bottom left). Unl=unloaded targets. (C, D) TCR-T or UT peripheral blood lymphocytes (PBL) were cocultured with B cells loaded with S100A11 peptides and blocking antibodies. Effector molecule production was quantified in cell coculture supernatants (C) and cell surface OX40 and 4-1BB expression was evaluated by flow cytometry (D).

TRAV6 and TRBV18 chains that recognized S100A11Q22R was identified via TCRb and single cell TCR sequencing. TRC-T were engineered with the full-length TCR sequence and cocultured with APCs bearing S100A11Q22R and S100A11WT peptide. The TCR-T produced high levels of effector cytokines (IFNg, TNFa, and Granzyme B), which was dependent on alignment of TCR, peptide, and MHC class II (figure 2C). Surface upregulation of 4-1BB, rather than OX40, governed this response for both CD4+ and CD8+ TCR-T (figure 2D). Despite CD8+ TCR-T activation, production of IFNg was not hindered by MHC class I blockade, suggesting that the CD8+ TCR-T cells directly recognized the peptide-MHC Class II complex independent of the CD8 coreceptor (data not shown).

Using the TCRb sequence, we tracked the CD4+ S100A11Q22R-specific clone throughout longitudinal patient peripheral blood samples to understand the persistence and trajectory of this clone during the patient's antitumor response. At infusion, this clone comprised 17% of the bulk TIL product, the second-most abundant clone at the time of ACT (figure 3A). After 1 week (W1), this clone expanded to become the most prevalent clone, at nearly 40% of the peripheral repertoire. Of the top ten clones in the infusion product, this represented the largest fold increase immediately after infusion, suggesting an initial clonal expansion. At W2, this clone maintained a 40% increase over its infusion frequency. After this time point, the endogenous T cell repertoire typically rebounds sharply from lymphodepletion, effectively diluting the frequency of adoptively transferred TIL.[73] Nevertheless, the S100A11Q22R-specific clone remained in the top 50 clones (45th) at least 6 weeks following infusion, indicating high persistence in the peripheral blood and suggesting a sustained response to this neoantigen during the patient's clinical response (figures 3B and 1B).

To further characterize this neoantigen-reactive CD4+ T cell clone and to better understand its relationship with other infused CD4+ TIL, tandem scRNASeq and TCRSeq were performed. Including Patient 1, the CD4+ TIL product from six metastatic melanoma patients were sequenced in this retrospective analysis, each previously treated with ACT on completed clinical trials at MCC. In total, 4903 CD4+ T cells were sequenced followed by unsupervised clustering (online supplemental figure 4A). Patient samples were distributed evenly across the UMAP and TCR expression was verified by VDJ recombination (online supplemental figure 4B,C). T cell clusters (C1–9) were annotated according to canonical gene modules and further characterized by the top differentially expressed genes (DEG) and genes previously reported to be enriched in neoantigen-specific CD4+ T cells (online supplemental figure 4D–F).[34–39 74]

Figure 3 Clonal analysis of neoantigen-specific CD4$^+$ TIL indicates persistence and effector profile. (A) TCRb sequencing of the infused TIL product for patient 1 displayed as relative productive frequency. Blue slice is the S100A11^{Q22R}-specific clone. (B) Relative productive frequency of the S100A11^{Q22R}-specific clone tracked longitudinally in PBMC samples at the indicated weeks (W) following TIL infusion. (C) Uniform manifold approximation and projection (UMAP) of the S100A11^{Q22R}-specific CD4$^+$ TIL clone (left) and the residual CD4$^+$ TIL (rCD4) from Patient 1. Cells were colored by clusters. (D) Relative frequency of the clusters displayed in figure 3C. (E) Scaled average expression of reported genes associated with neoantigen specificity in S100A11^{Q22R}-specific CD4$^+$ TIL and rCD4 TIL. Hierarchical clustering was performed on the selected genes and cell types. See online supplemental table 1 for the number of cells in each cluster. (F) Gene set enrichment analysis (GSEA) using DEG comparing S100A11^{Q22R}-specific CD4$^+$ TIL clone vs rCD4 from patient 1 across clusters. Normalized enrichment scores (NES) for pathway analysis were displayed. Hallmark, canonical pathways (CP) and gene ontogeny (GO) data sets were used. Full analysis in online supplemental materials.

Overall, ex vivo expanded CD4+TIL were highly similar and the S100A11^{Q22R}-specific CD4$^+$ TIL clone was widely distributed across the UMAP clusters, with the exception of C8 suggesting a lack of RORC+Th17 like cells. Despite this, the neoantigen-specific clonal profile was enriched for clusters C3, C5, and C9, consistent with T cells bearing an activated, cytotoxic and potentially exhausted program, when compared with the residual CD4$^+$ TIL (rCD4) from this patient (figure 3C,D). In addition, the S100A11^{Q22R}-specific CD4$^+$ TIL expressed genes derived from previously reported neoantigen-specific CD4$^+$ T cell signatures (figure 3E, online supplemental figure 4F and table 1).[34–39] Furthermore, this alignment with known markers of neoantigen reactivity was dictated primarily by the S100A11^{Q22R}-specific clone, rather than individual clusters, indicating high similarity between CD4$^+$ T cells within this clone and key transcriptional differences from rCD4 TIL. The hallmark clonal genes included *LAG3*, *IFNG*, chemokines and MHC class II molecules, which were significantly upregulated in comparison to rCD4 TIL (online supplemental figure 5). Gene set enrichment analysis (GSEA) revealed pathways involved in MHC class II antigen processing and presentation, IFNg signaling,

T cell cytotoxicity, and allograft rejection (figure 3F and online supplemental table 2). These modules were highly conserved across the clusters for the S100A11^{Q22R}-specific CD4$^+$ TIL clone in comparison to rCD4. Together, these data support the S100A11^{Q22R}-reactive CD4$^+$ TIL as a neoantigen specific, activated, effector T cell clone with cytotoxic capabilities, consistent with the functional activity of these CD4$^+$ TIL.

Patient 2

To determine whether neoantigen-specific CD4$^+$ TIL were present in other long-term responders to ACT with TIL, we investigated an additional metastatic melanoma patient treated with TIL. Patient 2's TIL product contained 88% CD8$^+$ T cells and efficiently eradicated the patient's tumor burden following ACT, resulting in a CR and PFS of 60 months (figure 4A,B). The bulk infusion product was highly reactive to AT in vitro; however, further interrogation demonstrated evidence of tumor-reactive CD4$^+$ TIL when preselected by IFNg secretion (online supplemental figure 6A–C).

Mutanome analysis of patient 2's tumor identified 1631 non-synonymous mutations, of which 147 neoantigen
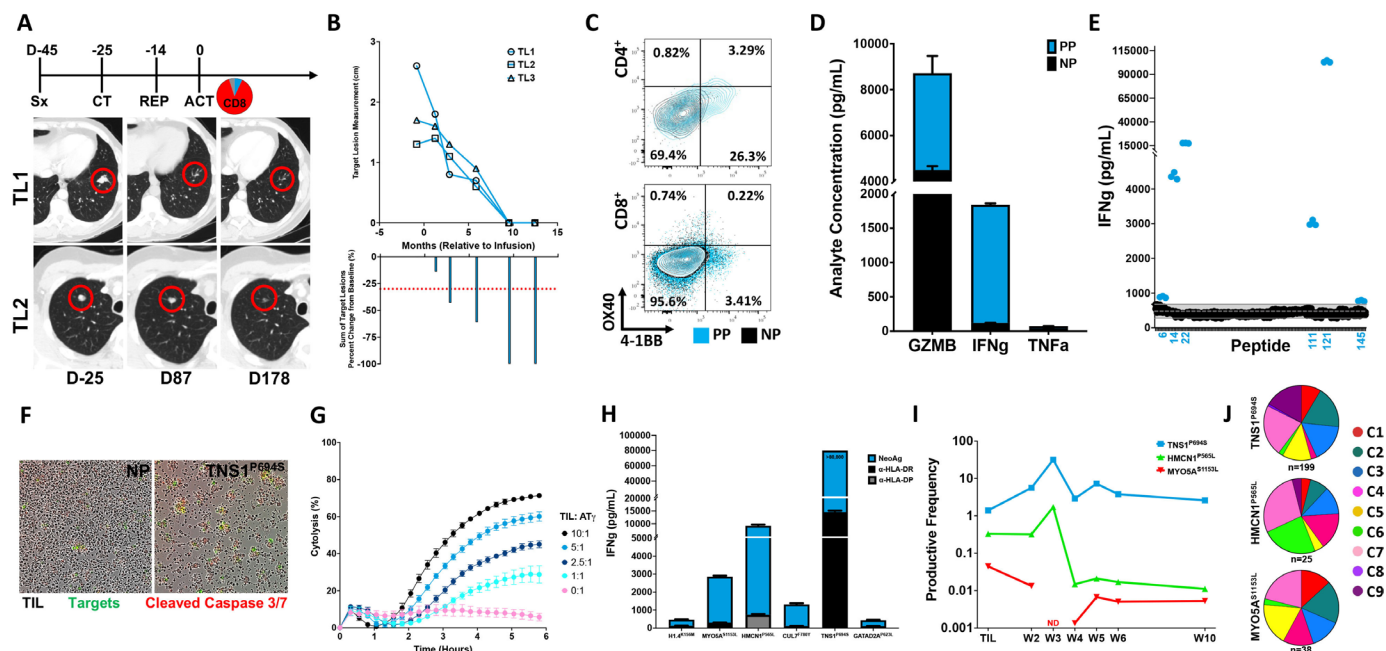
Figure 4 Multiple CD4+ TIL clones display distinct neoantigen reactivity. (A) Treatment course and CT images of target lesions (red circles) before and after therapy for patient 2. D=day (relative to TIL infusion), Sx=surgery, TL=target lesion. (B) Individual (upper) and sum (lower) measurements of target lesions by longest diameter for patient 2. Red dotted line indicates a –30% change from the baseline sum. (C) Bulk TIL and DC loaded with the neoantigen peptide pool (PP) or no peptide (NP) were cocultured followed by surface staining of OX40 and 4-1BB for cell sorting. (D) Bulk TIL production of granzyme B (GZMB), IFNg, and TNFa was analyzed in sort coculture supernatants. (E) Analysis of IFNg release by TIL in response to individual neoantigen peptides loaded onto APCs. Gray area were below threshold of reactivity. (F) TIL (unlabeled) and neoantigen-loaded target cells (green) were cocultured for 6 hours in a live cell imaging assay to capture cleaved caspase 3/7 (red) induction. Representative image displayed at 4 hours of coculture with 10:1 E:T. (G) Real-time cell-analysis (RTCA) of IFNg-pretreated autologous tumor (ATγ) following addition of neoantigen-specific CD4+ TIL. (H) APCs were loaded with neoantigen peptides, precoated with HLA-DR or HLA-DP blocking antibodies, and cocultured with neoantigen-specific CD4+ TIL. IFNg release was quantified by the Ella system for each condition. (I) Clonal tracking by TCRb sequencing of neoantigen-specific CD4+ TIL clones in the infused TIL product and PBMC at the indicated weeks (W).(J) Distribution of scRNASeq cell clusters present in neoantigen-specific CD4+ TIL clones, identified by TCRb sequence. PBMC, peripheral blood mononuclear cell.

peptides were synthesized and pulsed onto autologous APCs as a PP (online supplemental figure 6D). CD4+ TILs were preferentially activated as observed by 4-1BB and OX40 induction (figure 4C). As with patient 1, this corresponded with Granzyme B, IFNg, and TNFa secretion (figure 4D). TIL from patient 2 were sorted on upregulation of 4-1BB and OX40, which resulted in a dramatic population shift toward CD4+ TIL (NeoAg CD4) (online supplemental figure 6E). When the NeoAg CD4 were screened against each individual mutant peptide, six neoantigen 'hits' stimulated a robust CD4+ T cell activation via IFNg release, suggesting the presence of at least six neoantigen-reactive CD4+ TIL clones (figure 4E). Using live cell imaging, NeoAg CD4 TIL rapidly formed T cell-target complexes in vitro, resulting in induction of cleaved caspase 3/7 and dose-dependent elimination of MHC-II+ AT cells (figure 4F,G, online supplemental figure 6F). Each neoantigen response was efficiently abrogated in the presence of a pan-MHC Class II blocking antibody, five of which were found to be HLA-DR dependent (H1.4K156M, HMCN1P565L, CUL7F780Y, TNS1P694S, GATAD2AP623L), while one was HLA-DP dependent (MYO5AS1153L) (figure 4H).

In order to deconvolute the precise TIL clone and neoantigen pairs, we sorted each neoantigen-specific CD4+ TIL clone individually. We focused on the top three sorted clones, which comprised greater than 90% of the sum frequency of the NeoAg CD4 TIL. The TNS1P694S-specific clone represented the eighth-most prevalent clone in the infusion product. Following infusion, this clone increased in relative frequency to become the third-ranked clone at W2 and peaked at W3 as the top clone in the periphery, representing over 30% of the T cell repertoire. The TNS1P694S-specific clone continued to maintain relevance throughout the duration of the patient's response after this maximum, registering as the third-most prevalent clone in each subsequent peripheral blood draw through ten weeks. The HMCN1P565L-specific clone was the 24th ranked clone in the infusion product and similarly peaked at W3 as the 10th most prevalent clone in the periphery, marked by a fivefold expansion in relative abundance. The MYO5AS1153L-specific clone was the 120th ranked clone at time of infusion, peaked at W2, and preserved similar relative abundance at W10 (figure 4I). Summarily, neoantigen-reactive CD4+ TIL clones persisted in the patient's periphery and

demonstrated the ability to expand following infusion, suggesting clonal amplification and maintenance in response to antigen recognition.

Clonal analysis by scRNASeq demonstrated a strong presence of C3, C4, and C5 in each of the three neoantigen-specific CD4⁺ TIL clones (range: 32%–45%). These clusters were distinguished by genes indicative of activated effector and cytotoxic T cells, including *PRF1*, *GZMA*, *GZMH*, *GZMK*, and *NKG7*. As with patient 1, a broad distribution of TIL from each identified NeoAg CD4 clone was observed, including notable C2 and C7 clusters. Comparing NeoAg CD4 to CD4⁺ TIL sorted simultaneously for the absence of OX40 or 4-1BB induction (nCD4), again revealed that NeoAg CD4 TIL were distinct from their counterparts and enriched for a subset of genes associated with neoantigen-specific CD4⁺ T cells (online supplemental table 1 and figure 6G). Cytotoxicity-associated genes were present in both NeoAg CD4 and nCD4, predominantly in cluster C6, suggesting that additional CD4⁺ TIL capable of tumor cell lysis may also have been present within this sample. Overall, these data supported our in vitro functional data demonstrating that the NeoAg CD4 TIL clones displayed an effector T cell profile marked by CD4-mediated AT-directed cytotoxicity.

Patients 3 and 4

Next, we investigated whether neoantigen-reactive CD4⁺ TIL were present in the infusion product from patients who were non-responders to ACT with TIL. Patients 3 and 4 were each treated with predominantly tumor-reactive CD8⁺ TIL (97% and 58%, respectively) in the combination therapy setting (online supplemental figure 7A). Patient 3 reached stable disease with a PFS of 7 months, while patient 4 had a PFS of 10 months. We again pursued neoantigen identification from WES and RNASeq and evaluated the infused TIL from patients 3 and 4 for reactivity against 192 and 191 neoantigen peptides, respectively (online supplemental figure 7B).

Patient 3's TIL product contained both CD4⁺ and CD8⁺ neoantigen-specific TIL, yet a greater proportion of the CD4⁺ T cells were activated in response to the mutant PP (figure 5A). This corresponded with IFNg, TNFa, and Granzyme B secretion, indicating the presence of potent effector T cells capable of a cytotoxic response (figure 5B). Individual peptide screening uncovered four mutated neoantigen hits that each induced IFNg production from TIL (figure 5C). As CD4⁺ T cells were in the minority of the TIL product, we enriched for CD4⁺ TIL for further analysis (online supplemental figure 7C). Following CD4-enrichment, reactivity was
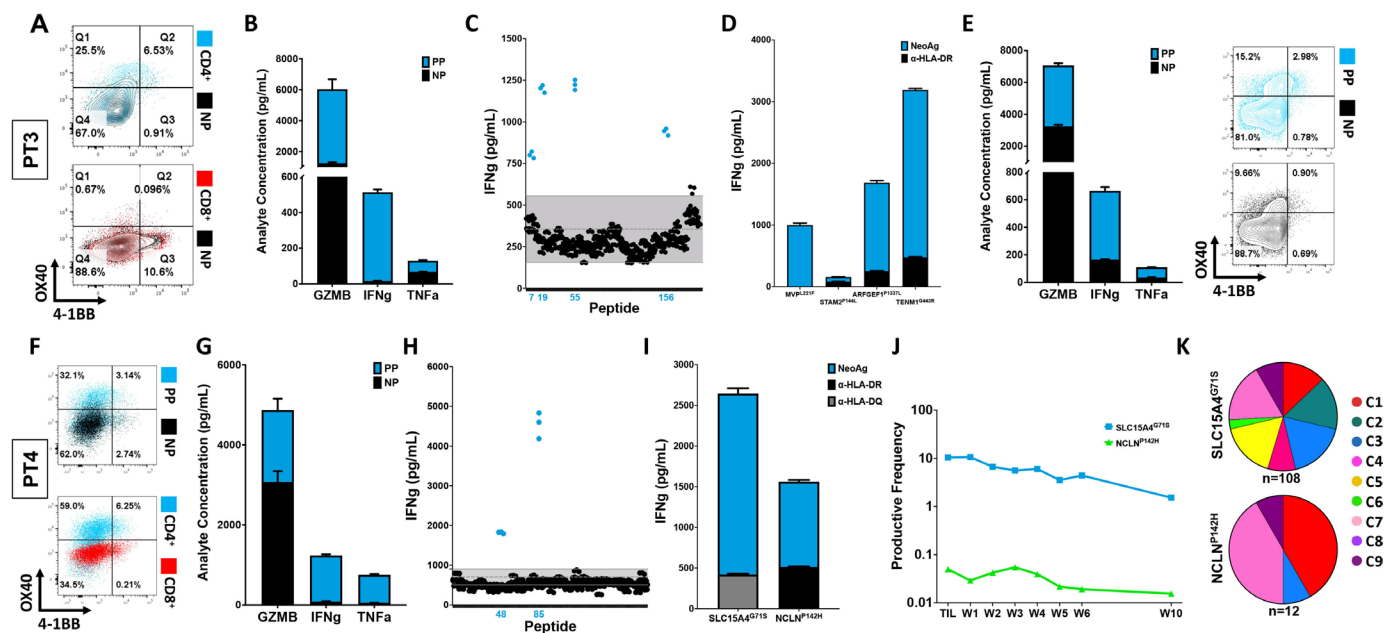
Figure 5 TIL product from non-responders contains neoantigen-specific CD4⁺ T cells. (A, F) Sorted neoantigen-specific TIL from patient 3 (A) and patient 4 (F) were cocultured with autologous B cells loaded with neoantigen peptide pool (PP) or no peptide (NP). OX40 and 4-1BB induction was analyzed by flow cytometry on the indicated T cell populations. B, G. Granzyme B (GZMB), IFNg, and TNFa were quantified in coculture supernatants from patient 3 (B) and patient 4 (G). C, H. Sorted TIL were validated for individual neoantigen peptide recognition by IFNg release following coculture with peptide-loaded autologous B cells, respectively, from patient 3 (C) and patient 4 (H). (D, I) Neoantigen peptide hits were loaded on autologous B cells, pretreated with the indicated blocking antibodies, then cocultured with neoantigen-specific CD4⁺ TIL to assess IFNg production from patient 3 (D) and patient 4 (I). (E) Effector molecule secretion and OX40 and 4-1BB induction on neoantigen-specific CD4⁺ TIL from patient 3 were quantified in response to AT-CIITA loaded with neoantigen peptide hits. (J) Clonal frequency of neoantigen-specific CD4⁺ TIL from patient 4 in the infused TIL product and PBMC at the indicated weeks (W) following ACT. (I) Frequency of the scRNASeq cell clusters presents within neoantigen-specific CD4⁺ TIL clones from patient 4. ACT, adoptive cell therapy; PBMC, peripheral blood mononuclear cell.

maintained in response to three of the four neoantigen peptide hits, indicating these responses were directed by CD4$^+$ T cells, while the response to STAM2^{P144L} was due to CD8$^+$ T cell reactivity. Blockade by pan-MHC class II and HLA-DR-specific antibodies confirmed that recognition of MVP^{L221F}, ARFGEF1^{P1337L}, and TENM1^{G443R} each occurred via CD4$^+$ T cell activation in the context of HLA-DR loaded with neoantigen peptide (figure 5D). To further investigate whether CD4$^+$ TIL were able to directly respond to the patient's tumor, we engineered the AT to enforce MHC class II expression using the Class II MHC transactivator (CIITA) construct. CD4$^+$ TIL responded to peptide-pulsed AT-CIITA via increased OX40 and 4-1BB expression on the cell surface as well as substantial effector molecule secretion, including the cytotoxic serine protease Granzyme B (figure 5E and online supplemental figure 4D). Altogether these data indicated that CD4$^+$ TIL from patient 3 were able to recognize and respond to neoantigens presented directly on MHC class II-competent tumor cells and APCs.

CD4$^+$ TIL also dominated the neoantigen response observed in Patient 4. In addition to robust effector molecule secretion, the majority of CD4$^+$ T cells upregulated OX40 and 4-1BB on mutant peptide stimulation (figure 5F,G). Following neoantigen-directed sorting, individual peptide screening indicated two neoantigen peptide hits (SLC15A4^{G71S} and NCLN^{P142H}) were responsible for the CD4$^+$ TIL stimulation (figure 5H). The CD4$^+$ T cell response was efficiently abrogated via HLA-DQ or HLA-DR blockade, indicative of the MHC class II component restriction for SLC15A4^{G71S} and NCLN^{P142H}, respectively (figure 5I). CD4$^+$ TIL were sorted for clonal enrichment in response to the individual neoantigen hits. Longitudinal clonal tracking of the two dominant sorted neoantigen-specific CD4$^+$ TIL clones showed relative stability in vivo after ACT followed by a moderate dilution in clonal frequency over time (figure 5J). Analysis by scRNASeq showed substantial C1 (*IL7R*), C3 (activated) and C7 (Th2-like) cluster presence within the profiles of each of these clones. Only the SLC15A4^{G71S}-specific CD4$^+$ clone clustered into C4 and C5, indicative of activated and cytotoxic T cells, although the relatively small clonal size of the NCLN^{P142H}-specific CD4$^+$ TIL clone may have influenced this cluster distribution (figure 5K). The effector profile and strong persistence of the SLC15A4^{G71S}-specific CD4$^+$ TIL suggested that this clone may have been therapeutically relevant following ACT, although overall this patient did not respond to the TIL infusion.

DISCUSSION

Investigation into the therapeutic use of TIL has predominantly focused on the administration of CD8$^+$ T cells, as ex vivo tumor reactivity is generally readily detectable in this population.[6 75] A comparison of the efficacy of CD8-enriched vs unselected TIL by Dudley *et al*, however, underscored that AT reactivity ultimately correlated with patient response rather than CD8$^+$ T cell frequency.[5]

The discovery of antigen-specific CD4$^+$ T cells within the tumor microenvironment and circulating in the periphery of cancer patients led to case studies examining their efficacy in ACT. While these studies reported impressive initial successes harnessing this T cell population, CD4$^+$ T cells remain an underexplored source of potent and capable antitumor effectors. Following the CR of a metastatic melanoma patient who was infused with an 88% CD4$^+$ TIL, we further studied the TIL product from additional metastatic melanoma patients previously treated with ACT to better understand the nature of neoantigen-specific CD4$^+$ TIL.

Using a series of case studies, we investigated the CD4$^+$ TIL compartment from four individuals previously treated with ACT using TIL at MCC, each having a varying response to therapy and composition of infusion product. We discovered between one and six previously undetected neoantigen-specific CD4$^+$ TIL clones, which recognized between 1% and 4% of screened neoantigens per patient, in line with other reports employing similar methodologies across multiple tumor types.[72 76 77] Notably, 12 of the 13 neoantigen-specific clones detected were CD4$^+$ T cells. Yossef *et al* found a similar dominance of neoantigen reactivity by CD4$^+$ T cells in metastatic epithelial cancer, suggesting that CD4$^+$ TIL may be predisposed to detection and response to this particular type of tumor antigen.[9] We were able to detect two of the identified neoantigen-specific CD4$^+$ TIL clones from patient 2 within that patient's tumor blocks, confirming their presence at 0.01% and 0.02% of the sequenced clones. Limitations in tissue quality and quantity prevented a robust analysis in this regard, however other groups have estimated that between 0.009% and 9.1% of TIL within the tumor represent neoantigen-reactive T cell clones.[34 78] The frequency of neoantigen-reactive T cells in the periphery is reportedly lower (0.002%–0.4%), underscoring that the endogenous tumor infiltrate represents an enriched source of tumor-specific T cells.[79] Improved sensitivity and detection methods will continue to expand the translational applications of neoantigen-reactive T cells in immunotherapy and may allow for less invasive isolation and expansion of these cells from biopsies and PBMCs or monitoring during treatment such as immune checkpoint blockade.

Tumor reactivity against AT and HLA-matched tumor was previously detected in the CD8-dominant TIL products of patients 2–4, suggesting that the CD8$^+$ T cells present may predominantly recognize shared antigens. While CD8$^+$ T cells have been historically associated with patient response in our patient set and across other institutions, 40% of our metastatic melanoma patients have received a TIL product comprised of greater than 40% CD4+T cells of unknown specificity. Current standards within the field are ineffective and inefficient in terms of identification and inclusion of antigen-specific CD4$^+$ T cells within traditional ACT products using TIL, compounded by the fact that CD4$^+$ T cells may have increased importance in non-melanoma solid tumors.

These circumstances reinforce the need to continue to develop strategies to investigate the presence and potential utility of antigen-specific CD4+TIL for ACT.

The identified neoantigen-specific CD4+ TIL responded to tumor antigens primarily via secretion of the effector molecules IFNg, TNFa, and Granzyme B. Additionally, these CD4+ TIL displayed direct antitumor cytotoxic capacity, which underscored their immense immunotherapeutic potential. We demonstrated that both MHC class II-competent tumor cells and APCs were able to efficiently induce an effector response from neoantigen-specific CD4+ TIL, indicating that each interaction may play a role in vivo during the T cell-mediated antitumor immune response. Endogenous or induced expression of MHC class II proteins represent readily available targets for tumor-specific CD4+ TIL and consequently a potential mechanism for direct tumor cell lysis. Oh and colleagues reported similar findings regarding the ability of CD4+ T cells isolated from bladder cancer to kill tumor cells in an MHC Class II and Granzyme B-dependent manner, as implicated in our present study.[36] In the absence of MHC class II expression on tumor cells, CD4+ T cells have been demonstrated to recognize tumor antigen directly via MHC class I and indirectly on APCs as potential alternative mechanisms of CD4+ T cell directed immunity. In the latter, CD4+ TILs are necessary components of a functional response to tumor antigens and initiate a broader immune response, including innate immune activation.[26 27 80 81] Current studies in our laboratory are focused on further defining which of these mechanisms may contribute following ACT in our metastatic melanoma patient cohort and other solid tumor populations.

Neoantigens were prioritized on expression at the RNA level and theoretical binding affinity to each patient's respective HLA molecules for practicality. As such, additional tumor-specific CD4+ TIL clones may have been present within the TIL product and potentially excluded. We demonstrated an ability to select and expand these neoantigen-specific CD4+ TIL based on induction of OX40 and 4-1BB, accepted markers of tumor antigen recognition.[15 72] Infusion of a TIL product enriched with neoantigen-specific CD4+ TIL would represent a highly personalized therapy, especially as all immunogenic mutations discovered here and across other studies were found to be unique.[72 77] Inclusion of neoantigen-specific CD4+ T cells into TIL products which already contain tumor-specific CD8+ T cells would effectively broaden the application of this therapeutic approach. Improved selection of TIL based on antigen recognition ensures a highly specific and potent T cell product and could potentially reduce the current standard of up to tens of billions of TIL for infusion. We also demonstrated that a neoantigen-reactive TCR isolated from CD4+ TIL can be used for generation of a highly potent TCR-T product. This represents an additional strategy for immunotherapeutic application of neoantigen-specific CD4+ T cells, with potentially broader implications depending on the antigen.

Clonal tracking revealed a rapid increase in relative frequency for the majority of analyzed neoantigen-specific CD4+ TIL clones in the periphery of patients following ACT. These data support the hypothesis that tumor-reactive CD4+ T cells underwent clonal expansion on recognition of cognate mutated peptides in vivo. This pattern was consistent between high and low frequency infused TIL clones, suggesting a functional response rather than homeostatic proliferation. Specifically in Patient 1, the CD4+ TIL clone that recognized S100A11^{Q22R} peaked at nearly 40% of the entire peripheral blood T cell repertoire. Coupled with substantial neoantigen expression in the resected tumor, a robust clonal CD4+ T cell effector profile, and a lack of detectable CD8+ T cell reactivity, we surmised that this neoantigen-specific clone contributed to the regression of this patient's tumors and resultant CR. Similarly, the infusion product for patients 2 and 4 contained neoantigen-specific CD4+ TIL clones that transiently increased in relative frequency, again suggesting antigen detection and expansion in vivo. Overall, the maintenance of tumor-reactive CD4+ T cell clones in the periphery following TIL transfer demonstrated persistence of these clones during a critical interval for therapeutic response. Persistence of transferred T cells has been implicated in positive outcomes for patients receiving ACT of TIL and CAR T Cells, including the detection of activated cytotoxic CD4+ T cells in long-term responders.[30 31 33] Future clinical studies which monitor T cell infiltration and tumor cell elimination at the respective clonal levels will help inform further mechanistic understanding of the processes involved in vivo at the tumor microenvironment. Additionally, infusion of tumor-reactive T cells does not preclude additional therapeutic resistance following ACT, which is an active area of research in our laboratory.[82]

Clonal analysis by scRNASeq supported the specificity and function of the discovered neoantigen-specific CD4+ TIL clones. Despite a high degree of inherent similarity in CD4+ TIL likely due to shared ex vivo conditions, the S100A11^{Q22R}-reactive CD4+ TIL from patient 1 demonstrated a profile marked by relative enrichment of activated and cytotoxic T cells as well as elevated transcripts previously reported as associated with neoantigen specificity.[34–39] Similarly, neoantigen-specific CD4+ clones isolated from patients 2 and 4 also clustered into activated effector T cell subsets, which corresponded with direct antitumor responses in vitro. In addition to cytolytic and cytokine gene modules, S100A11^{Q22R}-specific CD4+ TIL from patient 1 expressed high levels of LAG-3, MHC class II molecules, and chemokines. LAG-3 functions as a direct c-inhibitor for CD4+ T cells via impaired peptide-MHC class II interactions and is therefore a marker of antigen experience and tumor-specific T cells.[83 84] Targeting LAG-3 may serve as a strategy to release negative regulation and further enrich for neoantigen-reactive CD4+ T cells.[85 86] MHC class II and LAG-3 expression are also associated with T cell exhaustion possibly as a consequence of repeated antigen exposure, though relatively

few neoantigen-specific CD4^{+} TIL clustered into the exhausted state by scRNASeq.[74] Induction of MHC class II on CD4^{+} T cells has been previously observed following T cell activation and suggests that CD4^{+} TIL may be able to present MHC class II peptides.[87] The conditions and application of this potential mechanism require further interrogation but are supported by the GSEA data herein. Neoantigen-specific induction of chemokine production by CD4^{+} TIL indicated that these T cells have the potential to orchestrate a larger immune response, including attraction of CD8^{+} T cells, additional CD4^{+} T cells, DCs, and macrophages.[26 88 89] Surprisingly, we did not detect substantial expression of CXCL13 at the RNA level among our neoantigen-reactive CD4^{+} TIL clones, as recently reported, suggesting that tertiary lymphoid structure (TLS) formation may not be critical to the antitumor activity here.[34–39] Notably, the neoantigen-specific CD4^{+} TIL clones demonstrated a high degree of similarity between clusters, indicating a distinct profile of the neoantigen-specific CD4^{+} T cells when compared with other CD4^{+} T cell clones from the same patients. The wide distribution of neoantigen-specific CD4^{+} TIL across each of the observed clusters indicates that some degree of clonal heterogeneity or plasticity may exist to fulfill multiple niches within the tumor microenvironment on infusion. The optimal TIL product composition in terms of cell state and methodology to reproducibly generate these T cells ex vivo is an important ongoing area of investigation.[24] Our group is currently translating this work in an ongoing clinical trial (NCT05628883) that will continue to further the field of targeting both CD4 and CD8 neoepitopes.

We discovered previously undetected and uncharacterized clones of CD4^{+} TIL, which demonstrated evidence of neoantigen specificity and tumor reactivity. Our retrospective analysis supports a potential functional role for neoantigen-specific CD4^{+} TIL in patient responses to ACT and underscores the significance of identifying these cells for enrichment and inclusion in TIL infusion products. Future analyses which shed additional light on the mechanism and efficacy of these neoantigen-specific CD4^{+} T cells will be crucial to help determine their precise application in ACT with TIL, though mounting evidence indicates they can be a critical component of the antitumor immune response.

Author affiliations
[1]Department of Immunology, H. Lee Moffitt Cancer Center and Research Institute, Tampa, Florida, USA
[2]Cancer Biology PhD Program, University of South Florida, Tampa, Florida, USA
[3]Department of Biostatistics and Bioinformatics, H. Lee Moffitt Cancer Center and Research Institute, Tampa, Florida, USA
[4]Department of Cutaneous Oncology, H. Lee Moffitt Cancer Center and Research Institute, Tampa, Florida, USA
[5]Turnstone Biologics, Inc, San Diego, California, USA
[6]Molecular Genomics Core, H. Lee Moffitt Cancer Center and Research Institute, Tampa, Florida, USA
[7]Cell Therapies Core Facility, H. Lee Moffitt Cancer Center and Research Institute, Tampa, Florida, USA
[8]Department of Anatomic Pathology, H. Lee Moffitt Cancer Center and Research Institute, Tampa, Florida, USA
[9]Department of Sarcoma, H. Lee Moffitt Cancer Center and Research Institute, Tampa, Florida, USA

Provenance and peer review Not commissioned; externally peer reviewed.

Data availability statement Data are available on reasonable request. All data relevant to the study are included in the article or uploaded as online supplemental information. Sequencing data will be deposited in a controlled access repository according to accepted standards and complete pathway analyses made available with the publication. All additional data are available within this manuscript and its supplement or on reasonable request from the corresponding author.

Supplemental material This content has been supplied by the author(s). It has not been vetted by BMJ Publishing Group Limited (BMJ) and may not have been peer-reviewed. Any opinions or recommendations discussed are solely those of the author(s) and are not endorsed by BMJ. BMJ disclaims all liability and responsibility arising from any reliance placed on the content. Where the content includes any translated material, BMJ does not warrant the accuracy and reliability of the translations (including but not limited to local regulations, clinical guidelines, terminology, drug names and drug dosages), and is not responsible for any error and/or omissions arising from translation and adaptation or otherwise.

Open access This is an open access article distributed in accordance with the Creative Commons Attribution Non Commercial (CC BY-NC 4.0) license, which permits others to distribute, remix, adapt, build upon this work non-commercially, and license their derivative works on different terms, provided the original work is properly cited, appropriate credit is given, any changes made indicated, and the use is non-commercial. See http://creativecommons.org/licenses/by-nc/4.0/.

ORCID iDs
MacLean S. Hall http://orcid.org/0000-0002-5626-1619
Sebastian Snedal http://orcid.org/0000-0002-0771-7923
Ben Schachner http://orcid.org/0000-0001-9052-7575
James J. Mule http://orcid.org/0000-0001-7354-0516
John E. Mullinax http://orcid.org/0000-0002-9596-6785
Amod A. Sarnaik http://orcid.org/0000-0002-2337-5898

REFERENCES

1 Besser MJ, Shapira-Frommer R, Itzhaki O, *et al*. Adoptive transfer of tumor-infiltrating lymphocytes in patients with metastatic Melanoma: intent-to-treat analysis and efficacy after failure to prior Immunotherapies. *Clin Cancer Res* 2013;19:4792–800.
2 Pilon-Thomas S, Kuhn L, Ellwanger S, *et al*. Efficacy of adoptive cell transfer of tumor-infiltrating lymphocytes after Lymphopenia induction for metastatic Melanoma. *J Immunother* 2012;35:615–20.
3 Radvanyi LG, Bernatchez C, Zhang M, *et al*. Specific lymphocyte Subsets predict response to adoptive cell therapy using expanded Autologous tumor-infiltrating lymphocytes in metastatic Melanoma patients. *Clin Cancer Res* 2012;18:6758–70.
4 Rosenberg SA, Yang JC, Sherry RM, *et al*. Durable complete responses in heavily pretreated patients with metastatic Melanoma using T-cell transfer Immunotherapy. *Clin Cancer Res* 2011;17:4550–7.
5 Dudley ME, Gross CA, Somerville RPT, *et al*. Randomized selection design trial evaluating Cd8+-Enriched versus Unselected tumor-infiltrating lymphocytes for adoptive cell therapy for patients with Melanoma. *J Clin Oncol* 2013;31:2152–9.
6 Prieto PA, Durflinger KH, Wunderlich JR, *et al*. Enrichment of Cd8+ cells from Melanoma tumor-infiltrating lymphocyte cultures reveals tumor reactivity for use in adoptive cell therapy. *J Immunother* 2010;33:547–56.
7 Chacon JA, Sarnaik AA, Chen JQ, *et al*. Manipulating the tumor Microenvironment ex vivo for enhanced expansion of tumor-infiltrating lymphocytes for adoptive cell therapy. *Clin Cancer Res* 2015;21:611–21.
8 Mullinax JE, Hall M, Prabhakaran S, *et al*. Combination of Ipilimumab and adoptive cell therapy with tumor-infiltrating lymphocytes for patients with metastatic Melanoma. *Front Oncol* 2018;8:44.
9 Yossef R, Tran E, Deniger DC, *et al*. Enhanced detection of Neoantigen-reactive T cells targeting unique and shared Oncogenes for personalized cancer Immunotherapy. *JCI Insight* 2018;3:e122467.
10 Malekzadeh P, Yossef R, Cafri G, *et al*. Antigen experienced T cells from peripheral blood recognize P53 neoantigens. *Clin Cancer Res* 2020;26:1267–76.
11 Mautner J, Jaffee EM, Pardoll DM. Tumor-specific Cd4+ T cells from a patient with renal cell carcinoma recognize diverse shared antigens. *Int J Cancer* 2005;115:752–9.
12 Rosemblit C, Datta J, Lowenfeld L, *et al*. Oncodriver inhibition and Cd4(+) Th1 Cytokines cooperate through Stat1 activation to induce tumor Senescence and apoptosis in Her2+ and triple negative breast cancer: implications for combining immune and targeted therapies. *Oncotarget* 2018;9:23058–77.
13 Tempero RM, VanLith ML, Morikane K, *et al*. Cd4+ lymphocytes provide Muc1-specific tumor immunity in vivo that is undetectable in vitro and is absent in Muc1 transgenic mice. *J Immunol* 1998;161:5500–6.
14 Hunder NN, Wallen H, Cao J, *et al*. Treatment of metastatic Melanoma with Autologous Cd4+ T cells against NY-ESO-1. *N Engl J Med* 2008;358:2698–703.
15 Tran E, Turcotte S, Gros A, *et al*. Cancer Immunotherapy based on Mutation-specific Cd4+ T cells in a patient with epithelial cancer. *Science* 2014;344:641–5.
16 Zacharakis N, Chinnasamy H, Black M, *et al*. Immune recognition of somatic mutations leading to complete durable regression in metastatic breast cancer. *Nat Med* 2018;24:724–30.
17 Lu Y-C, Parker LL, Lu T, *et al*. Treatment of patients with metastatic cancer using a major Histocompatibility complex class II-restricted T-cell receptor targeting the cancer Germline antigen MAGE-A3. *J Clin Oncol* 2017;35:3322–9.
18 Cafri G, Yossef R, Pasetto A, *et al*. Memory T cells targeting Oncogenic mutations detected in peripheral blood of epithelial cancer patients. *Nat Commun* 2019;10:449.
19 Alspach E, Lussier DM, Miceli AP, *et al*. MHC-II neoantigens shape tumour immunity and response to Immunotherapy. *Nature* 2019;574:696–701.
20 Pearce H, Hutton P, Chaudhri S, *et al*. Spontaneous Cd4(+) and Cd8(+) T-cell responses directed against cancer Testis antigens are present in the peripheral blood of Testicular cancer patients. *Eur J Immunol* 2017;47:1232–42.
21 Janssen EM, Lemmens EE, Wolfe T, *et al*. Cd4+ T cells are required for secondary expansion and memory in Cd8+ T lymphocytes. *Nature* 2003;421:852–6.
22 Shedlock DJ, Shen H. Requirement for Cd4 T cell help in generating functional Cd8 T cell memory. *Science* 2003;300:337–9.
23 Ding Z-C, Huang L, Blazar BR, *et al*. Polyfunctional Cd4(+) T cells are essential for Eradicating advanced B-cell lymphoma after chemotherapy+ Polyfunctional Cd4(+) T cells are essential for Eradicating advanced B-cell lymphoma after chemotherapy. *Blood* 2012;120:2229–39.
24 Oja AE, Piet B, van der Zwan D, *et al*. Functional heterogeneity of Cd4(+) tumor-infiltrating lymphocytes with a resident memory phenotype in NSCLC. *Front Immunol* 2018;9:2654.
25 Mucida D, Husain MM, Muroi S, *et al*. Transcriptional Reprogramming of mature Cd4(+) helper T cells generates distinct MHC class II-restricted cytotoxic T lymphocytes. *Nat Immunol* 2013;14:281–9.
26 Haabeth OAW, Fauskanger M, Manzke M, *et al*. Cd4(+) T-cell-mediated rejection of MHC class II-positive tumor cells is dependent on antigen secretion and indirect presentation on host Apcs. *Cancer Res* 2018;78:4573–85.
27 Fauskanger M, Haabeth OAW, Skjeldal FM, *et al*. Tumor killing by Cd4(+) T cells is mediated via induction of inducible nitric oxide synthase-dependent macrophage cytotoxicity. *Front Immunol* 2018;9:1684.
28 Quezada SA, Simpson TR, Peggs KS, *et al*. Tumor-reactive Cd4(+) T cells develop cytotoxic activity and eradicate large established Melanoma after transfer into Lymphopenic hosts. *J Exp Med* 2010;207:637–50.
29 Xie Y, Akpinarli A, Maris C, *et al*. Naive tumor-specific Cd4(+) T cells differentiated in vivo eradicate established Melanoma. *J Exp Med* 2010;207:651–67.
30 Bailey SR, Nelson MH, Majchrzak K, *et al*. Human Cd26(High) T cells elicit tumor immunity against multiple malignancies via enhanced migration and persistence. *Nat Commun* 2017;8:1961.
31 Huang J, Khong HT, Dudley ME, *et al*. Survival, persistence, and progressive differentiation of Adoptively transferred tumor-reactive T cells associated with tumor regression. *J Immunother* 2005;28:258–67.
32 Lu YC, Jia L, Zheng Z, *et al*. Single-cell Transcriptome analysis reveals gene signatures associated with T-cell persistence following adoptive cell therapy. *Cancer Immunol Res* 2019;7:1824–36.
33 Melenhorst JJ, Chen GM, Wang M, *et al*. Decade-long leukaemia remissions with persistence of Cd4(+) CAR T cells. *Nature* 2022;602:503–9.
34 Lowery FJ, Krishna S, Yossef R, *et al*. Molecular signatures of antitumor Neoantigen-reactive T cells from metastatic human cancers. *Science* 2022;375:877–84.
35 Zheng C, Fass JN, Shih Y-P, *et al*. Transcriptomic profiles of Neoantigen-reactive T cells in human gastrointestinal cancers. *Cancer Cell* 2022;40:410–23.

36 Oh DY, Kwek SS, Raju SS, *et al*. Intratumoral Cd4+ T cells mediate anti-tumor cytotoxicity in human bladder cancer. *Cell* 2020;181:1612–25.

37 Cachot A, Bilous M, Liu Y-C, *et al*. Tumor-specific Cytolytic Cd4 T cells mediate immunity against human cancer. *Sci Adv* 2021;7:eabe3348.

38 Hanada K-I, Zhao C, Gil-Hoyos R, *et al*. A Phenotypic signature that identifies Neoantigen-reactive T cells in fresh human lung cancers. *Cancer Cell* 2022;40:479–93.

39 Veatch JR, Lee SM, Shasha C, *et al*. Neoantigen-specific Cd4+ T cells in human Melanoma have diverse differentiation States and correlate with Cd8+ T cell, macrophage, and B cell function. *Cancer Cell* 2022;40:393–409.

40 Aydin AM, Hall M, Bunch BL, *et al*. Expansion of tumor-infiltrating lymphocytes (TIL) from penile cancer patients. *Int Immunopharmacol* 2021;94:S1567-5769(21)00117-X.

41 Hall M, Liu H, Malafa M, *et al*. Expansion of tumor-infiltrating lymphocytes (TIL) from human Pancreatic tumors. *J Immunother Cancer* 2016;4:61.

42 Li H, Durbin R. Fast and accurate short read alignment with burrows-Wheeler transform. *Bioinformatics* 2009;25:1754–60.

43 DePristo MA, Banks E, Poplin R, *et al*. A framework for variation discovery and Genotyping using next-generation DNA sequencing data. *Nat Genet* 2011;43:491–8.

44 Cibulskis K, Lawrence MS, Carter SL, *et al*. Sensitive detection of somatic point mutations in impure and heterogeneous cancer samples. *Nat Biotechnol* 2013;31:213–9.

45 Saunders CT, Wong WSW, Swamy S, *et al*. Strelka: accurate somatic small-variant calling from sequenced tumor-normal sample pairs. *Bioinformatics* 2012;28:1811–7.

46 Wang K, Li M, Hakonarson H. ANNOVAR: functional annotation of genetic variants from high-throughput sequencing data. *Nucleic Acids Res* 2010;38:e164.

47 Dobin A, Davis CA, Schlesinger F, *et al*. STAR: Ultrafast universal RNA-Seq Aligner. *Bioinformatics* 2013;29:15–21.

48 Anders S, Pyl PT, Huber W. Htseq--a python framework to work with high-throughput sequencing data. *Bioinformatics* 2015;31:166–9.

49 Szolek A, Schubert B, Mohr C, *et al*. Optitype: precision HLA typing from next-generation sequencing data. *Bioinformatics* 2014;30:3310–6.

50 Bai Y, Wang D, Fury W. PHLAT: inference of high-resolution HLA types from RNA and whole Exome sequencing. *Methods Mol Biol* 2018;1802:193–201.

51 Jurtz V, Paul S, Andreatta M, *et al*. Netmhcpan-4.0: improved peptide-MHC class I interaction predictions integrating eluted ligand and peptide binding affinity data. *J Immunol* 2017;199:3360–8.

52 Reynisson B, Alvarez B, Paul S, *et al*. Netmhcpan-4.1 and Netmhciipan-4.0: improved predictions of MHC antigen presentation by concurrent motif Deconvolution and integration of MS MHC eluted ligand data. *Nucleic Acids Res* 2020;48:W449–54.

53 Hui-Yuen J, McAllister S, Koganti S, *et al*. Establishment of Epstein-Barr virus growth-transformed Lymphoblastoid cell lines. *J Vis Exp* 2011:3321.

54 Sarnaik A, Hall M, Mullinax J, *et al*. Clinical results of combined Vemurafenib and tumor-infiltrating lymphocyte therapy for metastatic Melanoma. *J Immunotherapy Cancer* 2015;3:S2.

55 Ramello MC, Benzaïd I, Kuenzi BM, *et al*. An Immunoproteomic approach to characterize the CAR Interactome and Signalosome. *Sci Signal* 2019;12:eaap9777.

56 Satija R, Farrell JA, Gennert D, *et al*. Spatial reconstruction of single-cell gene expression data. *Nat Biotechnol* 2015;33:495–502.

57 Wolock SL, Lopez R, Klein AM. Scrublet: computational identification of cell Doublets in single-cell Transcriptomic data. *Cell Syst* 2019;8:281–91.

58 McGinnis CS, Murrow LM, Gartner ZJ. Doubletfinder: doublet detection in single-cell RNA sequencing data using artificial nearest neighbors. *Cell Syst* 2019;8:329–37.

59 Germain P-L, Lun A, Garcia Meixide C, *et al*. Doublet identification in single-cell sequencing data using scDblFinder [version 1; peer review: 1 approved, 1 approved with reservations]. *F1000Res* 2021;10:979.

60 Lun ATL, McCarthy DJ, Marioni JC. A step-by-step Workflow for low-level analysis of single-cell RNA-Seq data with Bioconductor. *F1000Res* 2016;5:2122.

61 Hao Y, Hao S, Andersen-Nissen E, *et al*. Integrated analysis of Multimodal single-cell data. *Cell* 2021;184:3573–87.

62 Andreatta M, Corria-Osorio J, Müller S, *et al*. Interpretation of T cell States from single-cell Transcriptomics data using reference Atlases. *Nat Commun* 2021;12:2965.

63 Zheng L, Qin S, Si W, *et al*. Pan-cancer single-cell landscape of tumor-infiltrating T cells. *Science* 2021;374:6574.

64 Khan O, Giles JR, McDonald S, *et al*. TOX Transcriptionally and Epigenetically programs Cd8+ T cell exhaustion. *Nature* 2019;571:211–8.

65 Szabo PA, Levitin HM, Miron M, *et al*. Single-cell Transcriptomics of human T cells reveals tissue and activation signatures in health and disease. *Nat Commun* 2019;10:4706.

66 Aibar S, González-Blas CB, Moerman T, *et al*. SCENIC: single-cell regulatory network inference and clustering. *Nat Methods* 2017;14:1083–6.

67 Korotkevich G, Sukhov V, Budin N, *et al*. Fast gene set enrichment analysis. *Bioinformatics* [Preprint].

68 Godec J, Tan Y, Liberzon A, *et al*. Bhattacharya S, Butte AJ, Mesirov JP, Haining WN. compendium of immune signatures identifies conserved and species-specific biology in response to inflammation. *Immunity* 2016;44:194–206.

69 Subramanian A, Tamayo P, Mootha VK, *et al*. Gene set enrichment analysis: A knowledge-based approach for interpreting genome-wide expression profiles. *Proc Natl Acad Sci USA* 2005;102:15545–50.

70 Liberzon A, Subramanian A, Pinchback R, *et al*. Molecular signatures database (Msigdb) 3.0. *Bioinformatics* 2011;27:1739–40.

71 Liberzon A, Birger C, Thorvaldsdóttir H, *et al*. The molecular signatures database (Msigdb) hallmark gene set collection. *Cell Syst* 2015;1:417–25.

72 Parkhurst M, Gros A, Pasetto A, *et al*. Isolation of T-cell receptors specifically reactive with Mutated tumor-associated antigens from tumor-infiltrating lymphocytes based on Cd137 expression. *Clin Cancer Res* 2017;23:2491–505.

73 Innamarato P, Kodumudi K, Asby S, *et al*. Reactive Myelopoiesis triggered by Lymphodepleting chemotherapy limits the efficacy of adoptive T cell therapy. *Mol Ther* 2020;28:2252–70.

74 Anadon CM, Yu X, Hänggi K, *et al*. Ovarian cancer Immunogenicity is governed by a narrow subset of progenitor tissue-resident memory T cells. *Cancer Cell* 2022;40:545–57.

75 Dudley ME, Gross CA, Langhan MM, *et al*. "Cd8+ enriched "young" tumor infiltrating lymphocytes can mediate regression of metastatic Melanoma". *Clin Cancer Res* 2010;16:6122–31.

76 Parkhurst MR, Robbins PF, Tran E, *et al*. Unique neoantigens arise from somatic mutations in patients with gastrointestinal cancers. *Cancer Discov* 2019;9:1022–35.

77 Linnemann C, van Buuren MM, Bies L, *et al*. High-throughput EPITOPE discovery reveals frequent recognition of Neo-antigens by Cd4+ T cells in human Melanoma. *Nat Med* 2015;21:81–5.

78 Tran E, Ahmadzadeh M, Lu Y-C, *et al*. Immunogenicity of somatic mutations in human gastrointestinal cancers. *Science* 2015;350:1387–90.

79 Cohen CJ, Gartner JJ, Horovitz-Fried M, *et al*. Isolation of Neoantigen-specific T cells from tumor and peripheral lymphocytes. *J Clin Invest* 2015;125:3981–91.

80 Kruse B, Buzzai AC, Shridhar N, *et al*. Cd4(+) T cell-induced inflammatory cell death controls immune-evasive tumours. *Nature* 2023;618:1033–40.

81 Oliveira G, Stromhaug K, Cieri N, *et al*. Landscape of helper and regulatory Antitumour Cd4(+) T cells in Melanoma. *Nature* 2022;605:532–8.

82 Hall MS, Mullinax JE, Cox CA, *et al*. Combination Nivolumab, Cd137 Agonism, and adoptive cell therapy with tumor-infiltrating lymphocytes for patients with metastatic Melanoma. *Clin Cancer Res* 2022;28:5317–29.

83 Maruhashi T, Okazaki IM, Sugiura D, *et al*. LAG-3 inhibits the activation of Cd4(+) T cells that recognize stable pMHCII through its conformation-dependent recognition of pMHCII. *Nat Immunol* 2018;19:1415–26.

84 Matsuzaki J, Gnjatic S, Mhawech-Fauceglia P, *et al*. Tumor-infiltrating NY-ESO-1-specific Cd8+ T cells are negatively regulated by LAG-3 and PD-1 in human ovarian cancer. *Proc Natl Acad Sci U S A* 2010;107:7875–80.

85 Tawbi HA, Schadendorf D, Lipson EJ, *et al*. Relatlimab and Nivolumab versus Nivolumab in untreated advanced Melanoma. *N Engl J Med* 2022;386:24–34.

86 Goding SR, Wilson KA, Xie Y, *et al*. Restoring immune function of tumor-specific Cd4+ T cells during recurrence of Melanoma. *J Immunol* 2013;190:4899–909.

87 Mangalam A, Rodriguez M, David C. Role of MHC class II expressing Cd4+ T cells in Proteolipid Protein(91-110)-Induced EAE in HLA-Dr3 transgenic mice. *Eur J Immunol* 2006;36:3356–70.

88 Castellino F, Huang AY, Altan-Bonnet G, *et al*. Chemokines enhance immunity by guiding naive Cd8+ T cells to sites of Cd4+ T cell-Dendritic cell interaction. *Nature* 2006;440:890–5.

89 Kohli K, Pillarisetty VG, Kim TS. Key Chemokines direct migration of immune cells in solid tumors. *Cancer Gene Ther* 2022;29:10–21.